

Raman spectroscopy of Ryugu particles and their extracted residues: Fluorescence background characteristics and similarities to CI chondrites

Mutsumi KOMATSU ^{1,2*}, Hikaru YABUTA³, Yoko KEBUKAWA ^{4,5}, Lydie BONAL⁶, Eric QUIRICO⁶, Timothy J. FAGAN ², George D. CODY ⁷, Jens BAROSCH^{7,8}, Laure BEJACH⁹, Emmanuel DARTOIS¹⁰, Alexandre DAZZI¹¹, Bradley DE GREGORIO¹², Ariane DENISET-BESSEAU¹¹, Jean DUPRAT¹³, Cecile ENGRAND⁹, Minako HASHIGUCHI¹⁴, Zita MARTINS¹⁵, Jérémie MATHURIN¹¹, Gilles MONTAGNAC¹⁶, Smail MOSTEFAOUI¹³, Larry R. NITTLER^{7,17}, Takuji OHIGASHI¹⁸, Taiga OKUMURA¹⁹, Laurent RÉMUSAT¹³, Scott SANDFORD ²⁰, Rhonda STROUD ^{12,17}, Hiroki SUGA²¹, Yoshio TAKAHASHI¹⁹, Yasuo TAKEICHI²², Yusuke TAMENORI²¹, Maximilien VERDIER-PAOLETTI¹³, Shohei YAMASHITA²², Hisayoshi YURIMOTO ²³, Tomoki NAKAMURA²⁴, Takaaki NOGUCHI ²⁵, Ryuji OKAZAKI²⁶, Hiroshi NARAOKA²⁶, Kanako SAKAMOTO²⁷, Makoto YOSHIKAWA²⁷, Takanao SAIKI²⁷, Satoshi TANAKA²⁷, Fuyuto TERUI²⁸, Satoru NAKAZAWA²⁷, Tomohiro USUI²⁷, Masanao ABE²⁷, Tatsuaki OKADA²⁷, Toru YADA²⁷, Masahiro NISHIMURA²⁷, Aiko NAKATO²⁷, Akiko MIYAZAKI²⁷, Kasumi YOGATA²⁷, Shogo TACHIBANA ^{19,27}, Sei-ichiro WATANABE¹⁴, and Yuichi TSUDA²⁷

¹Division of Liberal Arts and Sciences, Saitama Prefectural University, Koshigaya, Saitama, Japan

²Department of Earth Sciences, Waseda University, Shinjuku, Tokyo, Japan

³Department of Earth and Planetary Systems Science, Hiroshima University, Hiroshima, Japan

⁴Department of Chemistry and Life Science, Yokohama National University, Yokohama, Japan

⁵Department of Earth and Planetary Sciences, Tokyo Institute of Technology, Meguro City, Tokyo, Japan

⁶Institut de Planétologie et d'Astrophysique, Université Grenoble Alpes, Grenoble, France

⁷Earth and Planets Laboratory, Carnegie Institution for Science, Washington, DC, USA

⁸School of Geosciences, University of Edinburgh, Edinburgh, UK

⁹Laboratoire de Physique des 2 Infinis Irène Joliot-Curie, Université Paris-Saclay, Centre National de la Recherche Scientifique, Orsay, France

¹⁰Institut des Sciences Moléculaires d'Orsay, Université Paris-Saclay, Centre National de la Recherche Scientifique, Orsay, France

¹¹Institut Chimie Physique, Université Paris-Saclay, Centre National de la Recherche Scientifique, Orsay, France

¹²Materials Science and Technology Division, US Naval Research Laboratory, Washington, DC, USA

¹³Institut de Mineralogie, Physique des Matériaux et Cosmochimie, Museum National d'Histoire Naturelle, Centre National de la Recherche Scientifique, Sorbonne Université, Paris, France

¹⁴Graduate School of Environmental Studies, Nagoya University, Nagoya, Japan

¹⁵Centro de Química Estrutural, Institute of Molecular Sciences and Department of Chemical Engineering, Instituto Superior Técnico, Universidade de Lisboa, Lisbon, Portugal

¹⁶École normale supérieure de Lyon, University Lyon 1, Lyon, France

¹⁷School of Earth and Space Exploration, Arizona State University, Tempe, Arizona, USA

¹⁸Institute for Molecular Science, UVSOR Synchrotron Facility, Okazaki, Japan

¹⁹Department of Earth and Planetary Science, The University of Tokyo, Tokyo, Japan

²⁰NASA Ames Research Center, Moffett Field, California, USA

²¹Japan Synchrotron Radiation Research Institute, Hyogo, Japan

²²Institute of Materials Structure Science, High Energy Accelerator Research Organization, Tsukuba, Japan

²³Department of Earth and Planetary Sciences, Hokkaido University, Sapporo, Japan

²⁴Department of Earth Science, Tohoku University, Sendai, Japan

²⁵Division of Earth and Planetary Sciences, Kyoto University, Kyoto, Japan

²⁶Department of Earth and Planetary Sciences, Kyushu University, Fukuoka, Japan

²⁷Institute of Space and Astronautical Science, Japan Aerospace Exploration Agency (JAXA), Sagami-hara, Japan

²⁸Kanagawa Institute of Technology, Atsugi, Japan

***Correspondence**

Mutsumi Komatsu, Division of Liberal Arts and Sciences, Saitama Prefectural University, 820 Sannomiya, Koshigaya, Saitama 343-8540, Japan.

Email: komatsu-mutsumi@spu.ac.jp

(Received 08 April 2023; revision accepted 16 June 2024)

Abstract—We present here an investigation of Ryugu particles recovered by the Hayabusa2 space mission and their extracted carbonaceous acid residues using Raman spectroscopy. Raman parameters of Ryugu intact grains and their acid residues are characterized by broad D (defect induced) and G (graphite) band widths, indicating the presence of polyaromatic carbonaceous matter with low thermal maturity. Raman spectra of Ryugu particles and CI (type 1) chondrites exhibit stronger laser-induced fluorescence backgrounds compared to Type 2 and Type 3 carbonaceous chondrites. The high fluorescence signatures and wide bandwidths of the D and G bands of Ryugu intact grains are similar to the Raman spectra observed in CI chondrites, reflecting the low structural order of their aromatic carbonaceous matter, and strengthening the link between Ryugu particles and CI chondrites. The high fluorescence background intensity of the Ryugu particles is due to multiple causes, but it is likely that the relative abundance of geometry-bearing macromolecular organic matter in total organic carbon contents makes a large contribution to the fluorescence intensities. Locally observed high fluorescence in the acid-extracted residues of Ryugu is due to nitrogen-bearing outlier phase. The high fluorescence signature is one consequence of the low degree of thermal maturity of the organic matter and supports evidence that the Ryugu particles have escaped significant parent body thermal metamorphism.

INTRODUCTION

Water-rich, hydrous asteroids are a diverse group of asteroids that experienced a range of aqueous alteration and thermal metamorphism. Primitive nebular materials in the early solar system were modified by secondary aqueous alteration and thermal metamorphism during/after planetesimal accretion (e.g., Alexander et al., 2017; Brearley, 2006). Thus, the hydrous asteroids record valuable information about the cosmochemical and geological evolution of small asteroids. The Hayabusa2 space mission investigated the surface of the C-type asteroid (162173) Ryugu for more than a year after rendezvousing with the asteroid in 2018 (Tsuda et al., 2020; Watanabe et al., 2019). Remote sensing observations of the surface showed that Ryugu was formed from an undifferentiated aqueously altered asteroid that may have experienced subsequent heating (Kitazato et al., 2019; Sugita et al., 2019). In December 2020, a total of about 5.4 g of material from the Ryugu surface was returned to Earth by Hayabusa2 (e.g., Tachibana et al., 2022). Ryugu is the fifth extraterrestrial body to be sampled by spacecraft, following previous sample return missions including Apollo, Luna, and Chang'e-5 samples from the Moon, GENESIS solar wind particles from the Sun, Stardust cometary dust from

Comet Wild 2, and Hayabusa samples from the near-Earth S-type asteroid Itokawa. Samples from a sixth extraterrestrial body, the asteroid Bennu, were collected by the OSIRIS-Rex mission, were returned to Earth in September 2023, and at the time of this writing, await detailed analyses and observations (Lauretta et al., 2022). Retrieved samples of the Hayabusa2 mission include materials from two touchdown sites of the surface and the sub-surface of Ryugu, the latter exposed by an artificial impact (Arakawa et al., 2020). Previous studies including curatorial studies and initial analyses on the returned samples have shown that the Ryugu samples are similar in mineralogy, textures, chemical composition, noble gas isotopic composition, and molecular and isotopic compositions of organic matter to CI (Ivuna-type) carbonaceous chondrites (Nakamura et al., 2022; Naraoka et al., 2023; Okazaki et al., 2022; Yabuta et al., 2023; Yokoyama et al., 2022). However, it is also suggested that Ryugu samples have different characteristics from CI chondrites including lower albedo, higher porosity (Yada et al., 2022), lack of sulfates and ferrihydrite, and low abundances of interlayer water in phyllosilicates (Nakamura et al., 2022; Yokoyama et al., 2022), a distinct oxidation degree (Amano et al., 2023), higher abundances of noble gases (Okazaki et al., 2022), partially low N isotopic

compositions (Naraoka et al., 2023; Okazaki et al., 2022; Yabuta et al., 2023), and high abundances of aromatic organic grains and diffuse organic matter (Yabuta et al., 2023).

Raman spectroscopy is an effective tool to acquire structural information on carbonaceous materials that reflect metamorphic histories and conditions. In particular, Raman spectra are used to examine peak metamorphic temperatures of host rocks of terrestrial (Ferrari & Robertson, 2000; Quirico, Rouzaud, et al., 2005) and extraterrestrial materials (Quirico, Borg, et al. 2005; Quirico et al., 2009; Wopenka, 1988). Many carbonaceous chondrites show the two first-order Raman bands of polyaromatic carbon materials, namely the D (“defect,” $\sim 1350\text{ cm}^{-1}$) and G (“graphite,” $\sim 1590\text{ cm}^{-1}$) bands and their width and peak positions are strongly related to the thermal processing their parent bodies have experienced (Bonal et al., 2006, 2007, 2016; Busemann et al., 2007; Quirico et al., 2003). Some carbonaceous chondrites exhibit a significant fluorescence signal in addition to Raman scattering (Busemann et al., 2007; Quirico, Borg, et al., 2005; Wopenka, 1988). We noticed that the Raman spectra of the Ryugu intact particles show significant laser-induced fluorescence as evidenced by high intensities of backgrounds under the Raman bands and high background slopes (Yabuta et al., 2023). Our interest lies in understanding the Raman fluorescence of Ryugu particles as well as D and G band characteristics, and evaluating whether fluorescence can be used as an independent indicator of thermal maturity of the Ryugu particles.

Here we present our investigation of Ryugu particles by Raman spectroscopy and through fluorescence signatures. We describe Raman spectra collected from intact Ryugu particles and extracted acid residues, and compare these results with Raman analyses from type 1, 2, and 3 carbonaceous chondrites to address: (1) whether the Raman spectra of Ryugu intact particles and their extracted residues show strong similarities with a specific chondrite group, and (2) whether the observed fluorescence of Ryugu particles can provide constraints on the degree of thermal metamorphism experienced by the asteroid Ryugu. This study builds on the Raman study of Ryugu particles reported by Bonal et al. (2024) by evaluating the effects of different laser powers on detected spectra and the role of fluorescence as a potential indicator of thermal maturity.

EXPERIMENTAL PROCEDURES

Samples

Raman point analyses were performed on five intact grains from Chamber A (A0106 #16, A0108 #5, #7, #17,

#58) and three from Chamber C (C0109 #1, #15, #16) aggregates, as well as one individual particle C0057 #3 from Chamber C. Extracted acid residues from Chamber A (A0106), Chamber C (C0107) aggregates and individual particle C0002 processed at Hiroshima University (Yabuta et al., 2023) were also examined (Tables 1 and 2). Chamber A and C samples were collected at the first and second touchdown sites, respectively. Chamber A samples were collected directly from the surface of Ryugu, whereas Chamber C samples were collected near an artificial impact crater after the small carry-on impactor had excavated material from the asteroid subsurface (Arakawa et al., 2020; Tachibana et al., 2022).

Pieces of Ryugu particles crushed on diamond windows were used for the measurements to ensure continuity with the FT/IR analysis in our coordinated study (Kebukawa et al., 2023). The particles were stored in a dry container before and after analyses to avoid terrestrial alteration with atmospheric water. We also studied the primitive carbonaceous chondrites Orgueil, Ivuna (type 1 CI chondrites), Tagish Lake, Tarda (C2-ungrouped), Murchison, Nogoya, and Jbilet Winselwan (type 2 CM chondrites), prepared similarly to the Ryugu intact grains. Polished thin sections of type 3 CV chondrites Leoville, Vigarano, and Allende were also examined. These carbonaceous chondrites were obtained from meteorite dealers and kept under vacuum to avoid atmospheric alteration before the Raman measurements. Petrologic types 1, 2, and 3 are attributed to reflect variable intensity of thermal metamorphism and/or aqueous alteration. Type 1 chondrites experienced complete aqueous alteration of anhydrous silicates, whereas the type 2 and 3 carbonaceous chondrites experiences high degree (type 2) or only incipient (type 3) hydration of silicates on their parent bodies. Type 3 chondrites used in this study experienced minor (Leoville and Vigarano) or moderate (Allende) thermal metamorphism (Bonal et al., 2006; Krot et al., 1995) that overlapped with or post-dated aqueous alteration (Bonal et al., 2020). Acid residues extracted from CM chondrite Murchison and produced at Hiroshima University (Yabuta et al., 2023) were also examined in this study.

Raman Spectroscopy Analyses

The Raman spectra were acquired with a Renishaw InVia Reflex Raman spectrometer equipped with 1800 lines per millimeter grating at the Materials Characterization Central Laboratory at Waseda University, using a 532 nm laser. The laser was focused on the sample surface out of a 50 \times objective with a spot size of approximately 3–4 μm . The maximum laser power was measured using the same objective: laser powers of 110 μW , 240 μW , and 1 mW at the surface were used in

TABLE 1. Average intensities in the Raman spectra from intact grains and extracted residues of Ryugu particles and meteorites.

Ryugu grains		Sample name	<i>n</i>	Average intensity at 1000 cm ⁻¹	SD	Laser power	
Intact grains	Chamber A	Aggregate A0106-16	9	131,408	31,862	1 mW	
		Aggregate A0108-5	10	157,684	34,787		
		Aggregate A0108-7	5	96,841	16,693		
		Aggregate A0108-17	14	108,563	20,097		
		Aggregate A0108-58	36	105,982	27,198		
	<i>Chamber A average</i>			116,271	63,105		
	Chamber C	Aggregate C0109-1	15	79,985	29,004		
		Aggregate C0109-15	14	136,680	29,004		
		Aggregate C0109-16	16	142,953	43,311		
		Individual particle C0057-3	14	83,600	39,270		
		<i>Chamber C average</i>			108,890		45,901
	Chamber A	Aggregate A0108-7	4	52,220	15,678	240 μW	
		Aggregate A0108-17	5	63,109	11,787		
		<i>Chamber A average</i>			58,270		14,687
Chamber C	Aggregate C0109-1	5	46,090	11,153			
	Aggregate C0109-15	4	49,723	6179			
	<i>Chamber C average</i>			47,705		9452	
Ryugu extracted acid residues	Chamber A	Aggregate A0106 residue #2	10	60,163	9617	110 μW	
		Aggregate A0106 residue #6	18	22,018	11,040		
		<i>Chamber A average</i>			41,090		19,072
	Chamber C	Aggregate C0107 residue #8	13	47,999	20,557		
		Aggregate C0107 residue #13	8	34,267	3318		
		Individual particle C0002	19	45,687	44,015		
		<i>Chamber C average</i>			41,263		31,567
Meteorites		Sample	<i>n</i>	Average intensity at 1000 cm ⁻¹	SD	Laser power	
Raw matrix	Type 1	Orgueil	18	54,355	33,337	1 mW	
		Ivuna	12	137,113	32,988		
	Type 1	Orgueil	15	119,441	37,970	240 μW	
		Ivuna	6	119,969	64,102		
	Type 2	Tagish Lake	3	15,134	1989		
		Tarda	5	19,757	2083		
		Murchison	6	13,368	3606		
		Nogoya	10	9694	2564		
		Jbilet Winselwan	13	9822	4979		
	Type 3	Leoville	7	1206	622		
		Vigarano	6	2196	226		
		Allende	4	1779	299		
	Extracted acid residues	Type 2	Murchison	11	14,449	3383	110 μW

the present study. Ideally, the same laser power would be used for all analyses; however, different laser powers were used to obtain sufficient signal-to-noise (S/N) while minimizing damage to the samples. Several test analyses

were conducted to evaluate the effects of different laser powers on detected Raman parameters and fluorescence intensities (see Supplemental Material). Test analyses of Ryugu grains show consistent variations in values

TABLE 2. Average Raman parameters and their SDs of the samples in this study.

	Sample name	<i>n</i>	ω_D (cm ⁻¹)	ω_G (cm ⁻¹)	FWHM _D (cm ⁻¹)	FWHM _G (cm ⁻¹)	I_D/I_G	Laser power ^b
<i>Ryugu intact grains</i>								
Chamber A	Aggregate A0106-16	9	1381.9 ± 4.9	1583.1 ± 3.1	253.4 ± 7.1	98.1 ± 2.8	0.67 ± 0.04	1 mW
	Aggregate A0108-5	10	1378.1 ± 4.8	1588 ± 6.2	251.9 ± 3.1	94.4 ± 1.9	0.66 ± 0.02	
	Aggregate A0108-7 ^a	5	1372.8 ± 1.7	1584 ± 3.6	236.1 ± 12.6	98.6 ± 3.9	0.68 ± 0.03	
	Aggregate A0108-17 ^a	14	1373.4 ± 5.6	1588.4 ± 3.7	232.1 ± 11.3	95.6 ± 4.9	0.76 ± 0.03	
	Aggregate A0108-58	36	1385.8 ± 8.7	1583.6 ± 3.7	248.2 ± 11.5	95.5 ± 2.5	0.69 ± 0.06	
	<i>Chamber A average</i>		1380.1 ± 9.2	1585.1 ± 4.6	243.7 ± 13.6	96.2 ± 3.8	0.7 ± 0.06	
Chamber C	Aggregate C0109-1 ^a	15	1382.0 ± 4.0	1580.9 ± 1.6	256.6 ± 10.7	98.7 ± 2.7	0.7 ± 0.05	
	Aggregate C0109-15 ^a	14	1380.5 ± 6.5	1585.6 ± 4.5	258.9 ± 7.0	96.2 ± 2.3	0.68 ± 0.02	
	Aggregate C0109-16	16	1380.1 ± 4.5	1582.1 ± 3.1	254.1 ± 11.5	100 ± 3.2	0.68 ± 0.05	
	Individual particle C0057-3	14	1377.9 ± 6.6	1582.9 ± 3.5	244.1 ± 14.3	98.2 ± 5.1	0.69 ± 0.08	
	<i>Chamber C average</i>		1380.2 ± 5.7	1682.8 ± 3.8	253.4 ± 12.6	98.4 ± 3.8	0.69 ± 0.05	
<i>Extracted acid residues</i>								
Chamber A	Aggregate A0106-2	10	1379.2 ± 8.0	1594.7 ± 4.2	186.7 ± 8.0	90.3 ± 6.1	0.74 ± 0.05	110 μW
	Aggregate A0106-6	15	1367.6 ± 5.7	1589.5 ± 6.9	221.4 ± 13.1	95.9 ± 4.0	0.7 ± 0.04	
	<i>Chamber A average</i>		1372.6 ± 8.6	1491.6 ± 6.4	206.4 ± 20.5	94.4 ± 6.4	0.7 ± 0.05	
Chamber C	Aggregate C0107-8	14	1370.2 ± 4.8	1590.8 ± 5.3	219 ± 10.5	97.3 ± 4.7	0.68 ± 0.02	
	Aggregate C0107-13	8	1367.4 ± 3.3	1589.8 ± 3.3	216.7 ± 7.1	94.6 ± 5.3	0.71 ± 0.01	
	Individual particle C0002	19	1372.3 ± 11.4	1589.5 ± 5.2	222.4 ± 24.5	95.8 ± 9.6	0.78 ± 0.1	
	<i>Chamber C average</i>		1370.6 ± 8.4	1589.9 ± 4.8	217.1 ± 14.1	95.8 ± 7.4	0.73 ± 0.08	
<i>Meteorite matrix</i>								
Type 1 (CI chondrites)	Orgueil	18	1372.8 ± 4.2	1580.2 ± 3.3	244.4 ± 4.2	96.8 ± 4.5	0.79 ± 0.07	1 mW
	Ivuna	12	1387.5 ± 5.4	1578.6 ± 2.4	239.5 ± 5.4	97.6 ± 1.2	0.7 ± 0.06	
Type 2	Tagish Lake	12	1372.6 ± 6.0	1583.7 ± 4.3	260.8 ± 6.0	90.7 ± 4.0	0.77 ± 0.05	240 μW
	Tarda	5	1370.9 ± 4.9	1586.7 ± 2.8	222.7 ± 4.9	98.9 ± 5.7	0.63 ± 0.04	
	Murchison	11	1361.3 ± 3.8	1591.8 ± 4.2	201.2 ± 11.4	90.6 ± 4.3	0.75 ± 0.04	
	Nogoya	10	1367 ± 2.7	1586.9 ± 4.8	213.1 ± 2.7	97.7 ± 6.4	0.7 ± 0.03	
	Jbilet Winselwan	13	1359.5 ± 8.3	1590.8 ± 5.4	209.1 ± 8.3	89.9 ± 4.8	0.83 ± 0.08	
Type 3 (CV chondrites)	Leoville	5	1351.7 ± 2.6	1600.4 ± 2.6	166.5 ± 5.7	74 ± 3.4	0.89 ± 0.06	
	Vigarano	6	1344.8 ± 2.2	1601 ± 2.2	134.6 ± 9.5	62.8 ± 3.8	0.86 ± 0.09	
	Allende	4	1349 ± 2.2	1601.7 ± 3.4	71.0 ± 6.6	61.7 ± 1.3	1.37 ± 0.06	
<i>Extracted acid residues</i>								
Type 2	Murchison	11	1363.2 ± 4.2	1591.1 ± 3.5	217.3 ± 6.8	86.0 ± 3.8	0.77 ± 0.02	110 μW

^aRaman parameters were calculated using fits to spectra with $R^2 \geq 0.96$. See Table S2 for parameters based on spectra analyzed at 240 μW with poorer quality fits.

^bRaman parameters of Ryugu intact grains, CI chondrites, and Tagish Lake meteorite were obtained from the Raman spectra measured at 1 mW laser, whereas the other meteorite samples were obtained with 240 μW. Extracted acid residues of both Ryugu samples and Murchison were measured with 110 μW laser.

of some Raman parameters (e.g., FWHM_D) detected using 240 μW versus 1 mW analyses (Figure S3). In general, however, differences in Raman parameters attributed to different laser powers are relatively minor compared to the distinct values characteristic of type 3

versus type 1 and 2 chondrites. In contrast, fluorescence intensities show mixed variations with laser power and decrease as repeated analyses are collected on the same spot (Supplemental Material and Results). In this study, the variable laser powers were used to determine Raman

parameters, whereas a constant laser power (240 μW) was used on fresh spots to compare fluorescence intensities (some 1 mW analyses also were collected; see [Results Section](#), Figure 2).

The spectrometer calibration was checked using a silicon standard at the beginning of each Raman analytical session. Each acquisition comprised five integrations of 10 s that were integrated to make the final spectrum. The Raman band positions (ω) are presented as wave numbers representing the Raman shift relative to the excitation laser wavelength. Peak positions for the D and G bands, their peak widths (measured as the full width at half maximum, FWHM), and intensities of the D versus G bands (I_D/I_G) were obtained for each individual spectrum. Multi-band fittings (e.g., D1, D2, D3, and D4) have been determined from Raman spectra of organic matter in some metamorphic rocks (Beysac et al., 2003; Homma et al., 2015; Kouketsu et al., 2014). However, two-band fittings have been used in several studies of C-rich materials in chondrites, and are effective for distinguishing variations in peak metamorphic temperatures in these rocks (Bonal et al., 2006, 2016, 2024; Busemann et al., 2007; Quirico et al., 2003). To maintain consistency with the data set of Raman parameters compiled from previous studies, we used two-band fittings in this study.

The analytical procedure follows two main steps (i) subtraction of the fluorescence backgrounds assuming a linear shape within the 900–1900 cm^{-1} range; (ii) fitting the D and G Raman bands with models consisting of a Lorentzian and Breit–Wigner–Fano profiles, respectively. Due to high fluorescence of Ryugu particles, the D and G bands in the spectra of some particles are hidden by the fluorescence background, resulting in a poor coefficient of determination (R^2). Therefore, we accepted only spectra that were successfully fitted with values of $R^2 \geq 0.96$. The position (ω), peak intensity, and FWHM of the D and G bands were determined for each spectrum. Average spectra were derived by averaging the spectra of approximately 5–20 points, depending on sample sizes, and average parameters are calculated as the average of individual parameters.

The Raman spectra we obtained in this study have prominent fringes in all wavelength ranges due to interference of the spectrometer (Figure 2 and Figure S1). The fringe interference is noticeable in the Ryugu samples and CI chondrites with high fluorescence background. In some high fluorescence spectra, interferences were high enough so that reliable Raman parameters could not be determined; however, in most cases, we found that the fringes had little effect on identifying and characterizing the D and G bands. As suggested by previous studies, absolute values of given Raman parameters vary depending on the measurement settings including the

design of the spectrometer and the fitting procedures (e.g., Busemann et al., 2007; Quirico et al., 2014). In this study, multiple laser powers were used for the examination of Raman spectra of Ryugu grains. A constant laser power of 240 μW was used to collect the Raman spectra that were used to compare fluorescence intensities of meteorite and Ryugu samples. However, different laser powers were used to collect spectra for the determination of Raman parameters; the challenge for these analyses was to obtain sufficient signal-to-noise and at the same time minimize sample damage. The effects of analytical conditions are discussed in the data supplement. The Raman analysis of the Organic Macromolecule Initial Analysis Team was performed by two groups, one from France (Bonal et al., 2024) and the other from Japan (this study). Both groups used the same laser wavelength and fitting procedures in the measurements for Ryugu particles and the results are generally consistent, though there are some variations in absolute values of detected Raman parameters. We present results from the Raman spectral study carried out in Japan, which includes the evaluation of the effects of different laser powers on Raman spectra and interpretation of fluorescence characteristics of Ryugu particles. Comparative analyses of Ryugu particles and type 1, 2, and 3 chondrites using a constant laser power (0.3 mW) led by the French team are reported in detail in Bonal et al. (2024) and are discussed during the presentation and interpretation of results of this study.

Intact grains and extracted acid residues were also studied on a JEOL IT-100LA scanning electron microscope (SEM) operating at 15 kV using back-scattered electron (BSE) imaging and energy dispersive spectrometer (EDS) at the Materials Characterization Central Laboratory at Waseda University. X-ray elemental maps of one intact grain and one acid residue were collected by SEM/EDS to characterize compositional variations. The elemental maps were collected by placing the samples on a diamond window and collecting X-rays in low-vacuum mode without carbon coating.

RESULTS

Ryugu Intact Grains

General Characteristics of Raman Spectra

The intact grains in this study consist mostly of dark, fine-grained, phyllosilicate-rich matrix and opaque grains including sulfides and Fe-oxide (Figure 1). Some transparent grains of various sizes are also present, which were identified by Raman analysis as carbonate (Figure 1e) or phosphate minerals (Figure 1f). Organic matter is associated with the matrix phyllosilicates.

Average Raman spectra of matrix areas of Ryugu intact grains are shown in Figure 2, together with those of

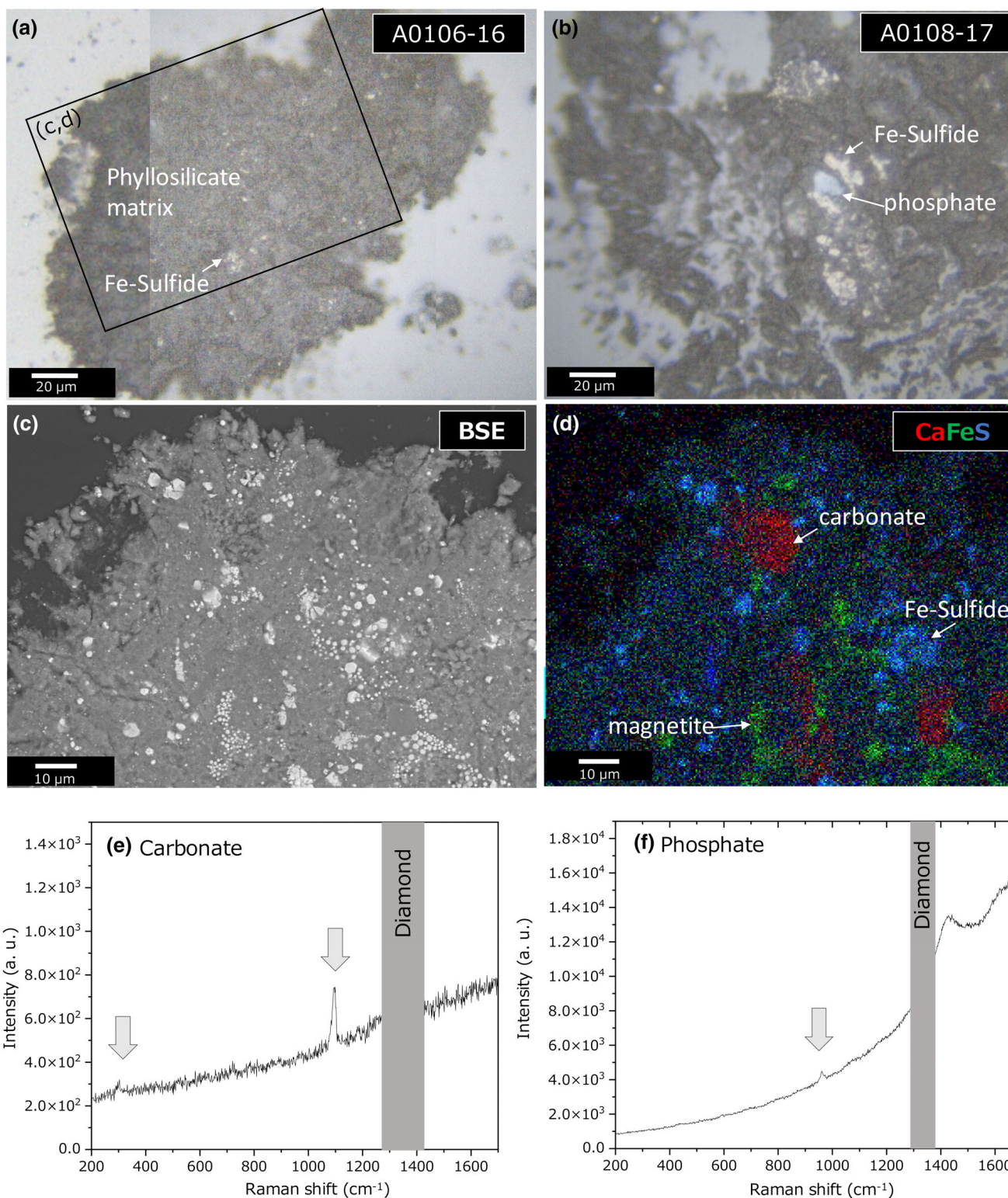


FIGURE 1. (a, b) Optical micrographs of intact grains of A0106-16 and A0108-17 pressed on the diamond window. (c, d) BSE image and combined X-ray elemental map (Ca = red, Fe = green, S = blue) of the enlarged area of the intact grain A0106-16, obtained after the Raman analyses. (e, f) carbonate grain labeled in (b) (measured at 240 μ W for 10 s) and phosphate grain labeled in (d) (A0106-16, measured at 1 mW for 10 s) were identified by Raman spectra. To make the mineral peaks visible, strong diamond peak (~ 1332 cm^{-1}) derived from the diamond window has been masked. (Color figure can be viewed at wileyonlinelibrary.com)

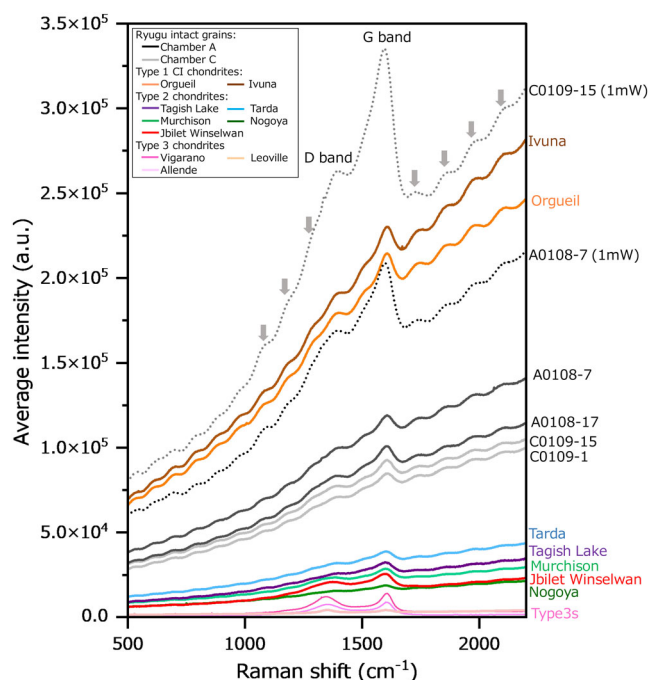


FIGURE 2. Average Raman spectra showing variations in fluorescence and fringes of Ryugu intact grains and carbonaceous chondrites. From 2 to 15 individual spectra were used to calculate the averages shown here (see Table 2). The carbonaceous chondrite spectra shown here were measured using the 240 μW laser power. Two Raman spectra of Ryugu intact grains A0108-7 and C0109-15 measured at 1 mW are also shown for comparison. Analyses with higher fluorescence background tend to have higher slopes and stronger fringes (indicated by arrows). (Color figure can be viewed at [wileyonlinelibrary.com](https://onlinelibrary.wiley.com))

the petrologic types 1, 2, and 3 carbonaceous chondrites, measured at a same laser power of 240 μW (two average spectra analyzed at 1 mW are shown for comparison). Analyses with higher fluorescence backgrounds tend to have higher slopes and stronger fringes (indicated by arrows in Figure 2). The fringes are well developed in spectra from the CI chondrites and Ryugu grains. For spectra collected at the same laser power (240 μW), the Ryugu grains have fluorescence intensities and slopes that are lower than the CI chondrites, but distinctly higher than the type 2 chondrites (Figures 2 and 3). The type 3 chondrites have the lowest fluorescence intensities, slopes, and fringes. The D and G bands are partially to completely masked by fluorescence and fringes in the spectra of Ryugu grains collected at 240 μW . The D band ($\sim 1350\text{ cm}^{-1}$) becomes more distinct when the laser power is increased to 1 mW (Figure 2).

Individual analyses within single grains exhibit variations in background intensities. Nevertheless, on average, the Ryugu intact grains have approximately four times higher fluorescence at 1000 cm^{-1} than CM chondrites (Table 1; Figure 3). In general, the

fluorescence intensities of the Ryugu intact grains measured at 240 μW fall between those observed in type 1 and type 2 chondrites. However, for analyses collected using laser power of 1 mW, fluorescence intensities at 1000 cm^{-1} of Ryugu grains overlap with those of CI chondrites (Table 1; Figure 3). We also observed a decrease in fluorescence intensities with increasing the petrologic types from type 2 to type 3, indicating there is a connection between the intensity of the fluorescence and the degree of thermal metamorphism. Because of the small number of grains analyzed, it is not possible to determine whether the higher fluorescence intensities of the Chamber A grains are due to random fluctuations between individual grains or if there is a systematic difference in fluorescence of Chamber A versus Chamber C grains.

Raman Parameters

The Raman parameters of Ryugu intact grains are characterized by wide D and G bandwidths, and generally overlap with those of type 1 and type 2 chondrites (Figure 4). The Ryugu intact grains from both Chambers A and C that we studied have Raman parameter values that overlap with those of CI chondrites. Compared to the type 2 chondrites, the Ryugu intact grains have similar I_D/I_G ratios, FWHM_G , ω_G , but the detected FWHM_D and ω_D values are slightly higher than those of the type 2 chondrites (Figure 4). However, the spectra collected for determining Raman parameters were collected at 240 μW for the type 2 chondrites other than Tagish Lake and at 1 mW for the Ryugu grains and Tagish Lake. As discussed in the Supplementary Material, test spectra of Ryugu grains collected using a laser power of 1 mW yielded FWHM_D values that were approximately 50 cm^{-1} higher than FWHM_D of 240 μW analyses (Figure S3). We note further that the FWHM_D of type 2 chondrite Tagish Lake, which was determined from 1 mW analyses, overlaps with those of the Ryugu grains (Figure 4b). Therefore, based on the data from this study, we infer that there are no significant differences between the Raman parameters of the Ryugu intact grains and the type 2 chondrites. Compared to the type 3 carbonaceous chondrites, the Ryugu intact grains have wider bandwidths for both the D and G bands, lower I_D/I_G , lower ω_G , and higher ω_D (Figure 4).

The similarity in Raman parameters of Ryugu particles to those of CI chondrites and unheated CM chondrites confirms the results of our companion study by Bonal et al. (2024). There are some differences in the values of the Raman parameters determined by the two groups. In particular, our values for the FWHM_D of the Ryugu intact grains are approximately 70 cm^{-1} wider than those of the French group (Figure 4; see figure 4 in

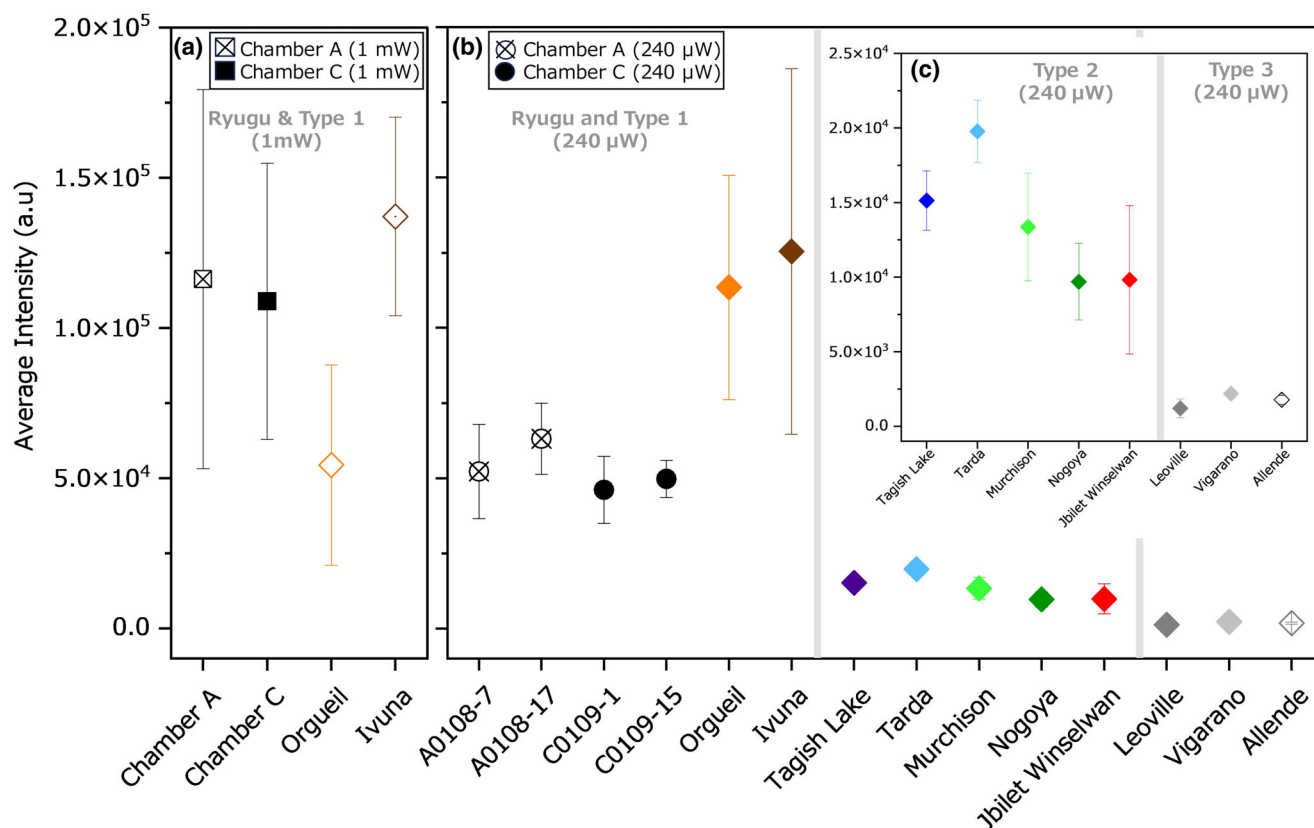


FIGURE 3. Comparison of average fluorescence intensities at 1000 cm^{-1} of Ryugu intact grains and carbonaceous chondrites: (a) Ryugu grains and CI (type 1) chondrites analyzed at 1 mW; (b) Ryugu grains and type 1, 2, and 3 carbonaceous chondrites analyzed at $240\text{ }\mu\text{W}$; (c) inset comparing fluorescence intensities of type 2 and type 3 carbonaceous chondrites in greater detail. Background fluorescence intensities of Ryugu intact grains and of CI chondrites overlap for the 1 mW analyses (a); however, for the $240\text{ }\mu\text{W}$ analyses, CI chondrites exhibit greater fluorescence than the Ryugu grains (b). Compared to both Ryugu grains and CI chondrites, type 2 and 3 carbonaceous chondrites have relatively low fluorescence (b). The type 3 chondrites analyzed in this study have lower fluorescence intensities than the type 2 chondrites (b, c). (Color figure can be viewed at [wileyonlinelibrary.com](https://onlinelibrary.wiley.com/doi/10.1111/maps.14234))

Bonal et al., 2024). However, the FWHM_D values of this study were determined from spectra collected at 1 mW, whereas the analyses of Bonal et al. (2024) were collected at 0.3 mW ; as discussed above, in the test analyses of this study, higher laser power analyses yielded wider FWHM_D (Figure S3). Thus, the discrepancy between the FWHM_D values of Ryugu intact grains of this study compared with the results of Bonal et al. (2024) is probably a consequence, at least in part, of the higher laser power used in this study.

A comparison of Raman parameters of type 1–3 chondrites obtained in this study with the results of the French group (Bonal et al., 2024) is shown in Figure S5. Orgeuil (CI type 1), Murchison and Nogoya (both CM2) were analyzed by both groups; several L/LL 3 chondrites were analyzed by Bonal et al. (2024), and CV 3 chondrites were analyzed in this study. Although several Raman parameters of corresponding meteorites determined by the two groups do not show 1:1 correlations, results from the two groups are consistent in

that: (1) Raman parameters determined from the type 1 and 2 meteorites cluster together; and (2) parameters of the type 3 meteorites are distinct from those of the type 1 and 2 in the same trends (e.g., I_D/I_G of the type 3 meteorites are higher than those of the type 1 and 2 meteorites based on analyses of both the French group and this study; see Figure S5e). Differences in equipment and analytical conditions (e.g., $300\text{ }\mu\text{W}$ used by Bonal et al. vs. $240\text{ }\mu\text{W}$ of this study, grains of type 3 chondrites analyzed by Bonal vs. thin sections analyzed in this study) combined with sample heterogeneities account for some of the differences in results of the two studies.

Acid Carbonaceous Residues from Ryugu Samples

The acid residues of Ryugu samples analyzed in this study have variable textures that were identified previously by Kebukawa et al. (2023) and Quirico et al. (2023). A dark-colored material similar to insoluble organic matter (IOM) extracted from type 1 and type 2

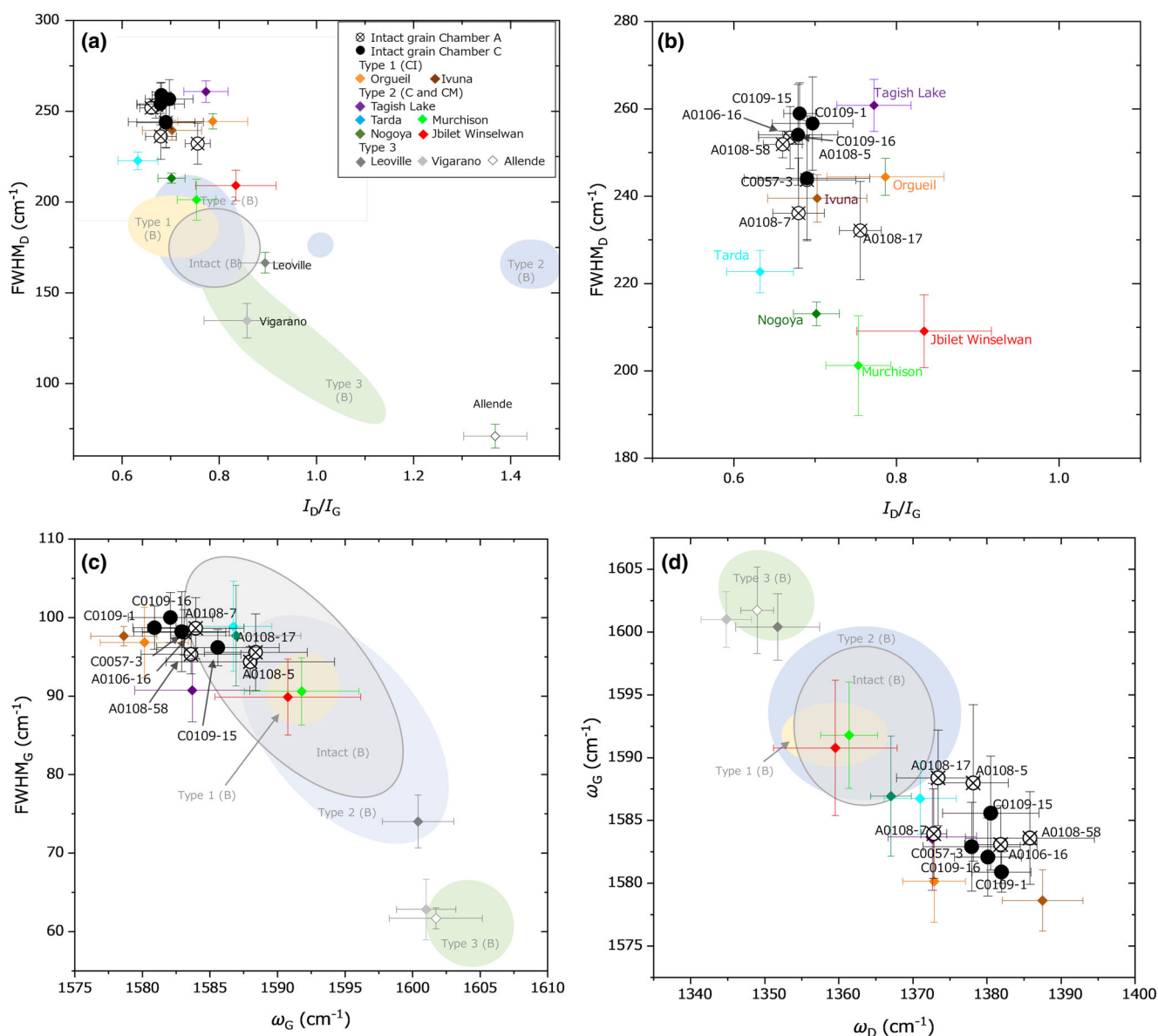


FIGURE 4. The Raman parameters of Ryugu intact grains and type 1, 2, and 3 carbonaceous chondrites. (a, b) Intensity ratio of D and G bands (I_D/I_G) versus full width at half maximum of D band ($FWHM_D$). The variation within the Ryugu intact grains is enlarged in (b). (c) G-band position (ω_G) versus full width at half maximum of G band ($FWHM_G$). (d) D band position (ω_D) versus G-band position (ω_G). Uncertainties are the SD of the mean values from each sample (1σ). Ryugu intact grains, type 1 CI chondrites, and Tagish Lake were measured at a laser power of 1 mW, while the other chondrites were measured at 240 μ W. Raman parameters obtained by the French team (Bonal et al., 2024) are shown for comparison; colored fields summarize the results of Bonal et al. (2024) for Ryugu intact grains (gray), type 1 (yellow), type 2 (blue), and type 3 chondrites (green). (Color figure can be viewed at [wileyonlinelibrary.com](https://onlinelibrary.wiley.com/doi/10.1111/rmap.14234))

carbonaceous chondrites was labeled “IOM-like” by Kebukawa et al. (2023; see Figure 5a,c). The other textural type is brownish in color and sticky during handling and was labeled “outlier phases” (Figure 5b). In some cases, distinct outlier phase material can be identified, but generally, the acid residues appear to be mixtures of the IOM-like and outlier phases. In addition to the fine-grained organic-rich materials,

Ni-rich Fe-sulfide, and elemental sulfur grains were identified in this study (Figure 5d and Figure S6).

Averaged Raman spectra of extracted acid residues of Ryugu samples from Chambers A and C, and Murchison measured using a laser power of 110 μ W are shown in Figure 6. Compared to the Ryugu intact grains, the acid residues have lower fluorescence backgrounds, allowing the separation of D and G

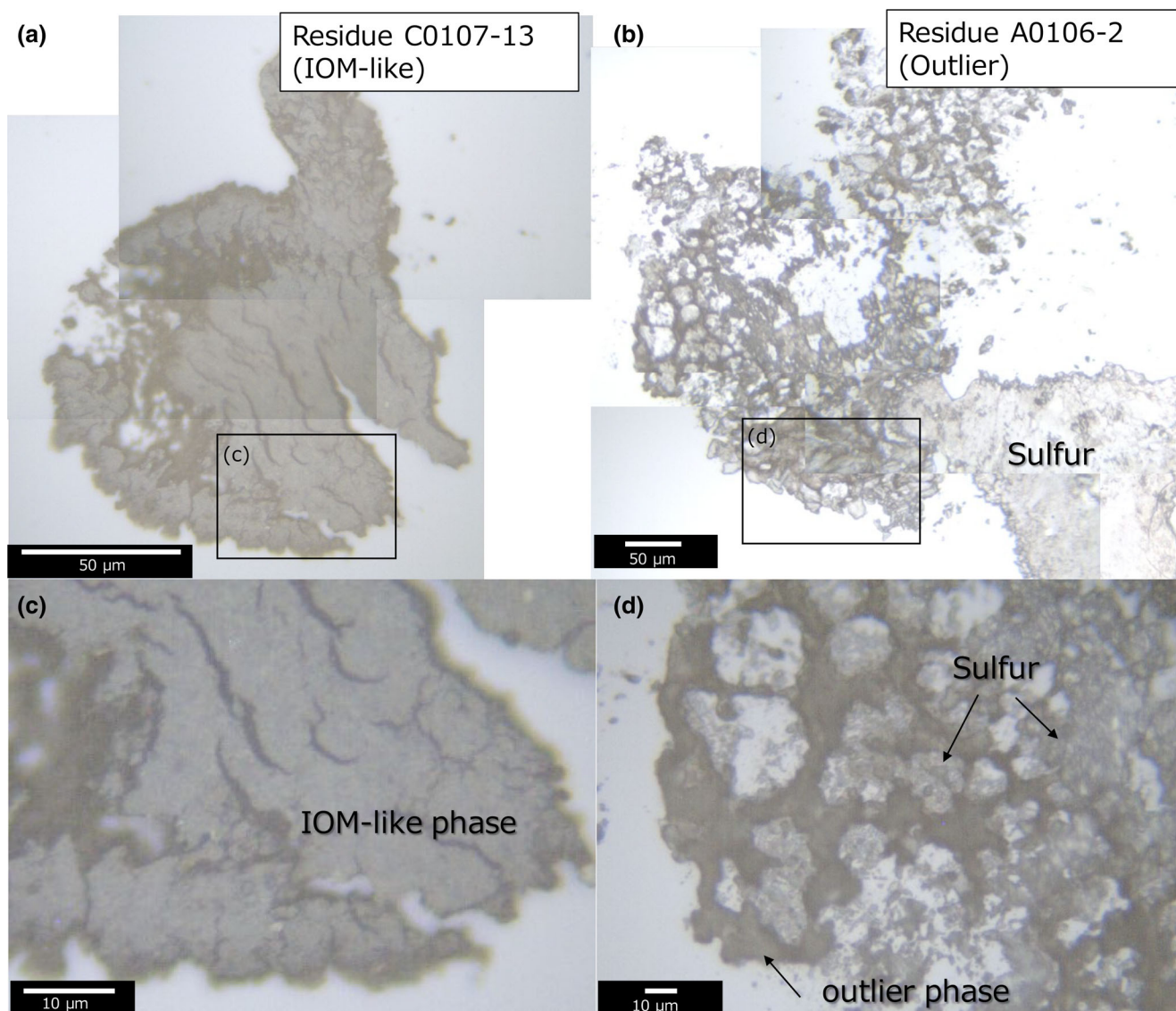


FIGURE 5. Optical micrographs of extracted acid residues of C0107-13 (a) and A0106-2 (b). The acid residues of Ryugu samples contain two texturally different phases of “IOM-like” and “outlier.” Residue C0107-13 is mainly composed of IOM-like phases (a), and residue A0106-2 consists of carbonaceous outlier phases and transparent grains (b). The IOM-like phases are comparable to the normal IOM extracted from type 1 and type 2 carbonaceous chondrites (c). In contrast, the outlier phases appear brownish and slightly glossy than IOM-like phases (d). (Color figure can be viewed at [wileyonlinelibrary.com](https://onlinelibrary.wiley.com/doi/10.1111/maps.14234))

bands from background even at low laser intensities (Tables 1 and 2; Figure S2a). In comparison, individual spectra from Murchison acid residues have both higher and lower fluorescence backgrounds than Murchison matrix, but the D and G bands are better developed in spectra of the acid residues (Figure S2b), allowing the bands to be identified at relatively low laser power analyses. Although the background intensities of individual analyses of the acid residues vary over a wide range, all of the average spectra of Ryugu acid residues have higher fluorescence than the acid residue of Murchison (Table 1; Figure 6).

Raman parameters of acid residues from Chambers A and C, together with the Murchison residue are shown in Figure 7. Raman parameters of intact grains obtained in this study, and extracted IOM of Ryugu grains and type 1 and 2 chondrites analyzed by Bonal et al. (2024), the meteoritic IOM by Busemann et al. (2007) and Starkey et al. (2013) are also shown. In general, Raman parameters determined in this study for the Ryugu acid residues overlap with those of the intact grains, though there are some subtle variations. The FWHM_D values of the residues tend to be slightly narrower, ω_G values higher and ω_D values lower than those of the intact

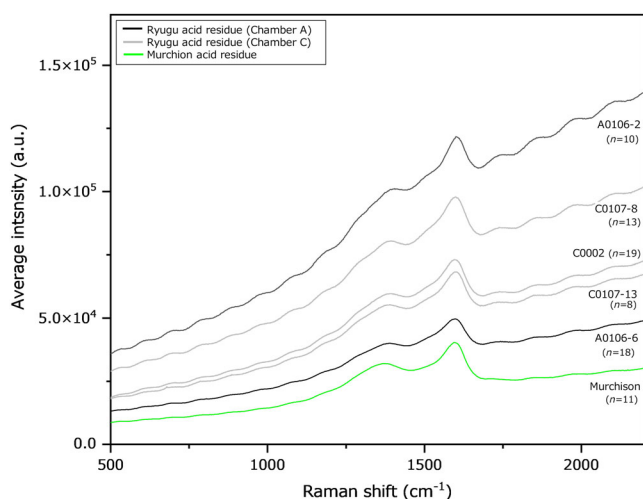


FIGURE 6. Averaged Raman spectra of the extracted acid residues of Ryugu samples (Chambers A and C) and Murchison. All spectra plotted here were collected using the same laser power ($110 \mu\text{W}$). The average fluorescence intensities of Ryugu acid residues are higher than those of Murchison. Note that the fluorescence background intensities of extracted acid residues are generally lower than those of intact grains (see Figure S2a). (Color figure can be viewed at wileyonlinelibrary.com)

grains (Figure 7). However, the acid residues were analyzed using a laser power of $110 \mu\text{W}$, whereas the intact grains were analyzed at 1 mW . As our test analyses show, differences in laser power may result in variations in detected Raman parameters (Figure S3); thus, the subtle variations in detected parameters of the acid residues versus intact grains should be viewed with caution. Most of the Raman parameters of acid residues of Ryugu grains and type 1 and 2 chondrites analyzed by Bonal et al. (2024) overlap with the analyses of this study (Figure 7); however, the FWHM_D values determined by Bonal et al., are narrower than the results of this study, possibly due to differences in analytical conditions.

The intact grains and acid residues of Ryugu grains and Murchison analyzed in this study have similar FWHM_D but low I_D/I_G compared to the acid residues of type 1 and 2 chondrites analyzed by Busemann et al. (2007; see Figure 7a). The FWHM_G and ω_G values of the Ryugu acid residues analyzed in this study are shifted to slightly higher values than those of the Busemann et al. (2007) type 1 and 2 chondrite residues, though within uncertainties for most analyses (Figure 7c). The Raman spectrometer settings used by Busemann et al. (2007) differ from the analytical conditions used for this study. Even so, the Raman parameters of the Ryugu acid residues share similarities with the acid residues of type 1 and 2 chondrites and are distinct from acid residues of the type 3 chondrites analyzed by Busemann et al. (2007; see Figure 7).

In this study, Raman spectra of the acid residues of Ryugu grains and Murchison were analyzed for G and D

band parameters and were used to evaluate fluorescence. The Raman parameters determined for the Ryugu samples and Murchison have overlapping values (Figure 7), but all of the Ryugu grain acid residues have higher average fluorescence intensities than that of the Murchison residue (Figure 6).

Variations of Raman Parameter of Ryugu Intact Grains and Extracted Acid Residues

Variations Within a Single Intact Grain

A single grain of A0108-58, $\sim 1 \text{ mm}$ in size, was crushed into multiple particles at Yokohama National University, and Raman spectra were collected separately as the interior and surface of the original grain. In order to help understand possible changes related to space weathering or solar irradiation heating on the surface of Ryugu on individual grains, we compared the Raman spectra of the interior and surface of grain A0108-58. A 1 mW laser power was used for these analyses; the average fluorescence at 1000 cm^{-1} and Raman parameters of this grain are shown in Tables 1 and 2, respectively. The fluorescence background intensities of individual spectra vary widely, and there is no significant difference between the interior and surface analyses (Figure S7a). In addition, the Raman parameters of both the interior and surface grains show wide ranges of values (Figure S7b–d). Spectra from the grain interior show a wider scatter of band parameters, but most analyses from the interior and surface have overlapping values. No major variations in the Raman signatures were observed between the surface and interior analyses of A0108-58.

The surface on the asteroid Ryugu was exposed to interplanetary space and was irradiated by solar wind and bombardment from high-velocity micrometeoroids, resulting in space weathering on the surfaces of some grains (Noguchi et al., 2023a, 2023b). The effects of space weathering include amorphization of silicates, and some Ryugu particles (6%–7% in $<100\text{-}\mu\text{-sized}$ grains; $\sim 66\%$ in large grains) are found to show evidence of space weathering (Noguchi et al., 2023a, 2023b). In addition, solar radiative heating (Sugita et al., 2019) could have caused structural changes in organic matter on the surface of Ryugu. Our observations could indicate that the A0108-58 grain originated from a larger particle and that its surface has not been subjected to intense space weathering or solar heating. However, considering that space weathering alters only a thin region of the surface ($\sim 100 \text{ nm}$ according to Noguchi et al., 2023a, 2023b), this may suggest that the effects of space weathering are difficult to detect with point Raman analysis. A comprehensive smaller scale analysis would be required to discuss a structural variation related to asteroid surface alteration.

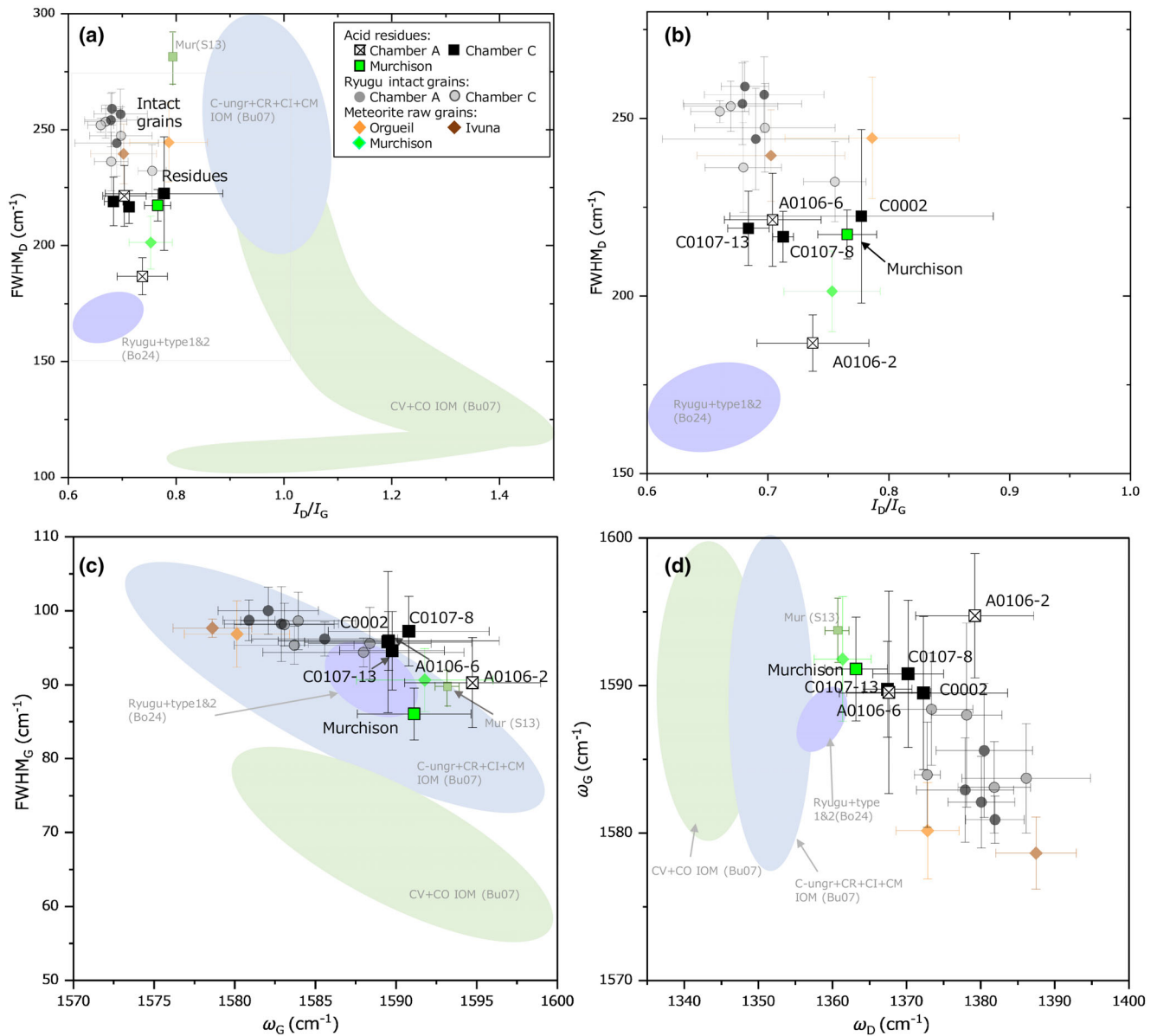


FIGURE 7. Raman parameters of the extracted acid residues from Ryugu raw grains A, C, and Murchison. (a, b) I_D/I_G versus $FWHM_D$. (c) ω_G versus $FWHM_G$. (d) ω_D versus ω_G . The acid residues were measured at 110 μW , whereas intact grains were measured at different laser powers (240 μW for Murchison, 1 mW for Ryugu intact grains, and type 1 CIs). Raman parameters of intact grains (this study) and literature data from Bonal et al. (2024), Busemann et al. (2007), and Starkey et al. (2013) are also shown for comparison. The Raman parameters of the extracted residues from Ryugu, type 1 and type 2 chondrites by Bonal et al. (2024) exhibit similar values and plot in the small area colored in purple (labeled as Bo24). The field colored in blue represents IOM from C-ungrouped, CR, CI, and CM chondrites (labeled as “C-ungr+CR+CI+CM IOM (Bu07)”) and green field represents IOM from CV and CO chondrites (labeled as “CV+CO IOM (Bu07)”) from Busemann et al. (2007). The green square plots labeled as “Mur (S13)” represent the Raman parameters of Murchison from Starkey et al. (2013). Note that different laser powers were used in the literature; 0.3 mW for Bonal et al. for 2024, $\sim 55 \mu W$ for Busemann et al. (2007), and $< 70 \mu W$ for Starkey et al. (2013). (Color figure can be viewed at [wileyonlinelibrary.com](https://onlinelibrary.wiley.com))

Variations Within the Extracted Acid Residue

Similar to the Ryugu intact grains, extracted acid residues also exhibit a wide range of fluorescence (Figures 2 and 6). In acid residues of grain C0107, spectra collected from the outlier phase exhibit higher

fluorescence and greater heterogeneity in fluorescence than in the IOM-like phase (Figure 8). The same is true of outlier versus IOM-like phases in residues extracted from grain C0002 (Figure S8). In comparison, spectra collected from residues of Murchison (IOM-like) have

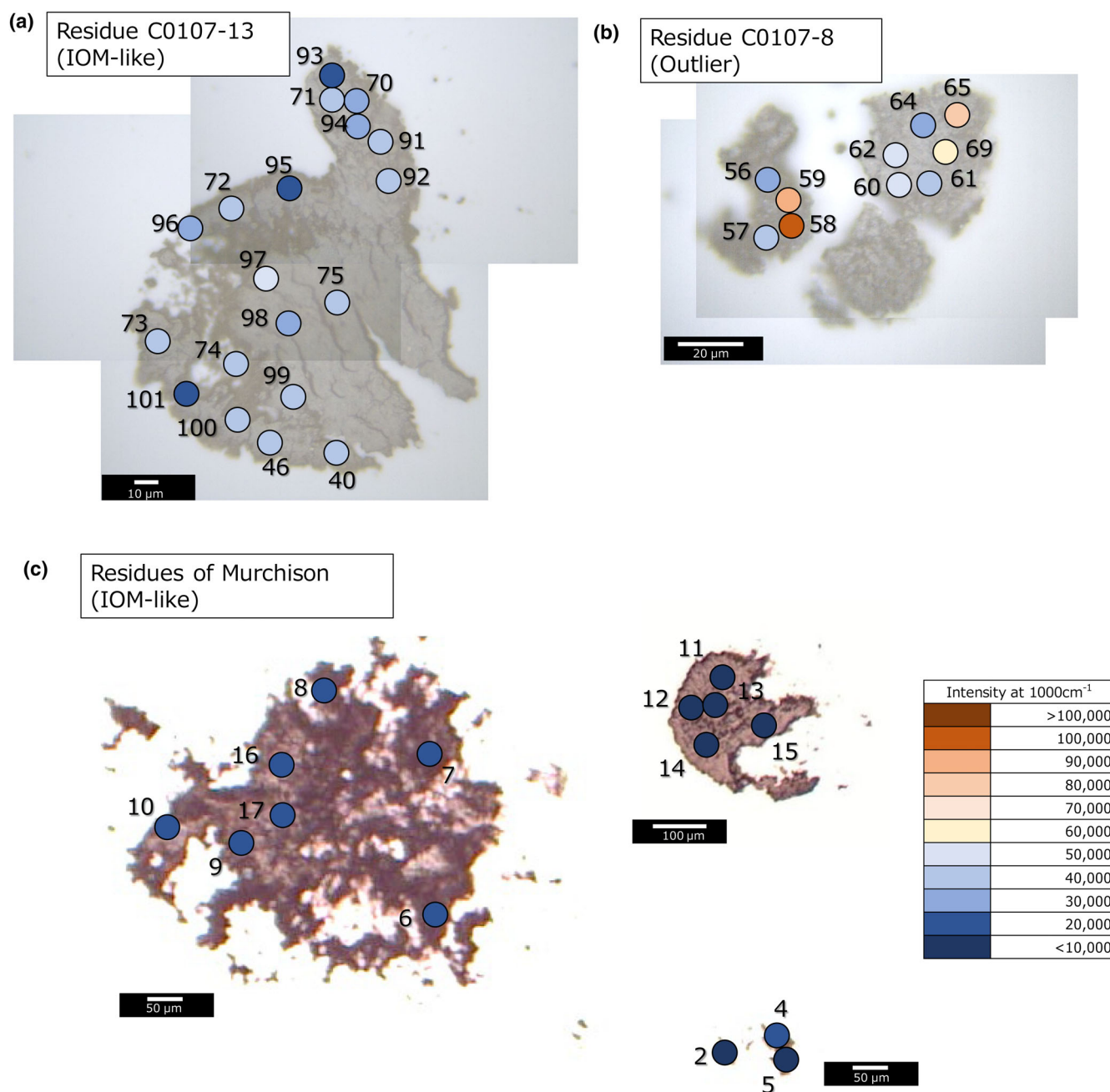


FIGURE 8. Optical micrographs of “IOM-like” residue C0107-13 (a) and “outlier” residue C0107-8 (b), and Murchison residues (c). The spectra collected from residues of Murchison (IOM-like) have lower fluorescence and are more homogeneous in fluorescence than the acid residues from Ryugu samples. The spots on the samples are shown to represent the intensity at 1000 cm^{-1} of the Raman spectra, and the numbers indicate the original analysis numbers. The actual analytical spot size is 3–4 μm . (Color figure can be viewed at wileyonlinelibrary.com)

lower fluorescence and are more homogeneous in fluorescence than the Ryugu acid residues (Figure 8).

Raman parameters of individual spectra were calculated for acid residues of Ryugu grain C0002; however, parameters were calculated only for spectra with relatively low fluorescence (intensity at $1000\text{ cm}^{-1} < 60,000$ counts for $110\text{ }\mu\text{W}$ analyses) because

the D and G bands are masked in spectra with higher fluorescence (Figure S8). In the fluorescence intensity range where Raman parameters were successfully obtained (the spots colored blue in Figure S8), no clear relationship between fluorescence intensity and Raman parameters was observed. It should also be noted that the outlier and IOM-like phases are present as mixtures and

cannot be completely separated (Kebukawa et al., 2023), the difference in Raman parameters could be masked by the mixing of two phases.

DISCUSSION

Implications of the Raman Spectra of Ryugu Particles

Aqueous Alteration and Thermal Processing

Raman spectra of Ryugu particles show high fluorescence backgrounds that are distinct from type 2 and 3 chondrites (Figures 2 and 3), indicating some differences in structures and/or compositions of organic matter of Ryugu grains versus type 2 and 3 chondrites (see [Possible Causes for the Fluorescence of Raman Spectra](#) Section). High fluorescence backgrounds similar to those of the Ryugu particles occur in the type 1 chondrites Ivuna and Orgueil. Raman spectra were also collected from extracted acid residues of the Ryugu particles and of the CM2 chondrite Murchison. Similar to data from the intact grains, all of the averaged spectra from the Ryugu acid residues have higher fluorescence backgrounds than that of Murchison (Figure 6). The high fluorescence intensities of Ryugu grains (both intact particles and acid residues) relative to most type 2 CM chondrites are consistent with the results of our companion study (Bonal et al., 2024). The Ryugu acid residues exhibit ranges of fluorescence intensities, in terms of both averages from different residue grains (Figure 6) and individual analyses in single grains (Figure 8). The greater intensities and heterogeneities of fluorescence backgrounds of spectra from the Ryugu acid residues compared to the Murchison acid residue may be connected to varying ratios of IOM-like phases versus outlier phases in organic matter of the Ryugu particles (Kebukawa et al., 2023; Quirico et al., 2023).

Similar to the variations in fluorescence, the Raman parameters FWHM_D , I_D/I_G , FWHM_G , ω_G and ω_D of the Raman intact particles are distinct from the Raman parameters of the CV3 chondrites Leoville, Vigarano and Allende analyzed in this study and of the type 3 ordinary chondrites analyzed by Bonal et al. (2024; Figure 4). The relatively high FWHM_D and low I_D/I_G of the Ryugu grains in particular indicate that the Ryugu grains have lower thermal maturities than type 3 chondrites. Raman parameters from the extracted residues also are distinct from those of the type 3 chondrites analyzed by Busemann et al. (2007) and suggest relatively low thermal maturities of Ryugu grains (Figure 7). The Raman parameters of Ryugu intact grains and acid residues determined in this study overlap with or are somewhat shifted from the Ryugu samples analyzed by Bonal et al. (2024) and the type 1 and 2 chondrites analyzed in previous studies (Bonal et al., 2024; Busemann

et al., 2007; Starkey et al., 2013; see Figures 4 and 7). As discussed in Results and in the data supplement, the discrepancies between these data sets are probably due to differences in analytical conditions (laser power in particular) and heterogeneities in the samples.

Taken together, the fluorescence backgrounds and Raman parameters determined in this study indicate that the Ryugu grains have low thermal maturities, similar to the thermal maturities of type 1 and 2 chondrites, consistent with the results of Bonal et al. (2024). However, the thermal histories and peak temperatures of type 1 and type 2 chondrites are difficult to evaluate in detail, partly because of brecciation and re-assembly of clasts of different subtypes in the same chondrite (e.g., Lentfort et al., 2021) and partly because of their complex thermal histories, including short-term, localized thermal excursions during impact events (e.g., Nakamura, 2005; Quirico et al., 2018; Velbel & Zolensky, 2021). Quirico et al. (2018) demonstrated that heated type 2 chondrites exhibit slightly different Raman parameters than unheated type 2 chondrites. They classified R1 (unheated), R3 (moderately heated, I_D/I_G lower than in R1), and R2 (heated; I_D/I_G higher and FWHM_D lower than in R1) subgroups based on Raman parameters and found a general correlation with the heating categories of Nakamura (2005), which are based mostly on X-ray diffraction and TEM-scale textural indicators of dehydration.

In this study, we have compared the Raman spectra of the heated type 2 CM chondrite Jbilet Winselwan with spectra from unheated CM2 chondrites, CV3 chondrites, and the Ryugu samples. Jbilet Winselwan is a breccia proposed as one of the CM chondrites, containing lithologies that suffered thermal metamorphism at 400–500°C after aqueous alteration, likely due to impact heating (King et al., 2019), or the early onset of aqueous alteration and subsequent thermal metamorphism at >300°C due to the decay of short-lived radionuclides (Fujiya et al., 2022). Based on our results, the average fluorescence intensity of Jbilet Winselwan is as high as other unheated type 2 chondrites (Figures 2 and 3). In addition, Raman parameters of Jbilet Winselwan are not significantly different from the unheated type 2 chondrites that we analyzed (Figure 4). However, the spectral valley between D- and G-band is deep compared to the spectra of the unheated type 2 chondrites (Figure 2), consistent with moderate heating of CM chondrites (classification R3 of Quirico et al., 2018), as discussed in Bonal et al. (2024). Although we did not perform petrologic examination of our Jbilet Winselwan sample, it is likely our sample is classified as moderately heated type 2 (R3), or mixture of unheated and moderately heated type 2 lithologies. The mixing of lithologies is consistent with the observation that Jbilet Winselwan is a breccia and contains lithologies with variable secondary alteration degrees (Friend et al., 2018).

Heterogeneities in the Extracted Acid Residues of Ryugu Particles

Heterogeneities in the physical appearance and IR spectra of acid residues extracted from Ryugu particles have been described in studies by Kebukawa et al. (2023) and Quirico et al. (2023). In both of these studies, extraction of IOM from Ryugu grains yielded a dark material similar to IOM extracted from carbonaceous chondrites (IOM-like) and a distinct brown to yellow translucent material (outlier carbonaceous phases). IR spectra of the IOM-like material are not uniform, but in general, they exhibit similarities to spectra of IOM extracted from type 1 and 2 carbonaceous chondrites (Kebukawa et al., 2023; Quirico et al., 2023). In contrast, spectra from the outlier phases are distinct from chondrite IOM. Kebukawa et al. (2023) classified the acid residues into three phases: (i) a phase with IR spectra like typical insoluble organic matter (IOM-like); (ii) an outlier phase with characteristic N-bearing IR absorption; and (iii) an outlier phase lacking distinct N-related IR features. The outlier IR spectra have not been observed in carbonaceous chondrites, but are found in Ryugu samples A0106, C0107, C0002, and A0108 (Kebukawa et al., 2023; Quirico et al., 2023).

Based on our Raman analyses, the outlier phases have relatively high and heterogeneous fluorescence intensities compared to the IOM-like phases in Ryugu samples (Figure 8a,b). The fluorescence intensities of the Murchison acid residues are lower and more homogeneous than those of the IOM-like and outlier phases of the Ryugu samples (Figures 6 and 8). Among the extracted residues examined in this study, the A0106-2 residue is composed primarily of outlier phases (Figure 5b). The average fluorescence intensity of A0106-2 residue is higher than those of the other residues (Figure 6). In addition, the outlier phase-rich residue A0106-2 has slightly different Raman parameters (higher ω_D and ω_G , and narrower FWHM_D) compared to the other residues (Figure 7). The relatively narrow FWHM_D is consistent with greater thermal maturity in the transition from type 2 to type 3 chondrites. However, the type 3 chondrites analyzed in this study have lower fluorescence than type 2 chondrites, suggesting a general correlation between higher metamorphic temperatures and lower fluorescence intensities (Figures 2 and 3; also see Bonal et al., 2016). Therefore, if the narrow FWHM_D of the A0106-2 residue is a consequence of relatively high metamorphic temperature, one implication is that variations in fluorescence intensities depend on other controls in addition to temperature.

It has been suggested that high fluorescence intensities might be caused by high N/C ratios (Wopenka et al., 2013) and by low CH₂/CH₃ (Muñoz Caro et al., 2006). Kebukawa et al. (2023) reported that the A0106-2 residue

has N-related IR features with a relatively high CH₂/CH₃ peak intensity ratio. Increases in CH₂/CH₃ ratio are usually attributed to thermal processing (Kebukawa et al., 2023; Quirico et al., 2018 and references herein). In the case of the A0106-2 acid residue, one Raman feature (FWHM_D) and one IR feature (CH₂/CH₃) point toward a relatively high-temperature origin (typically, low fluorescence), and the IR spectra collected by Kebukawa et al. (2023) indicates significant N abundance. In this case, the effect of high N concentration might compensate for the relatively high-T origin, resulting in high fluorescence of the A0106-2 acid residue.

Possible Causes for the Fluorescence of Raman Spectra

Chemical Compositions of Organic Matter

We observe a negative correlation between the fluorescence intensities in Raman spectra and degree of long-term thermal metamorphism. Indeed, it has been suggested in previous studies that fluorescence background decreases in thermally metamorphosed type 3 chondrites (e.g., Bonal et al., 2016). Considering that the low fluorescence intensities of thermally metamorphosed type 3 chondrites are related to the low H/C ratios of IOM (< ~0.4) (Busemann et al., 2007; Muñoz Caro et al., 2006), the high intensities of fluorescence in Ryugu particles observed in this study may be at least partially controlled by relatively high H/C ratios of organic matter, consistent with low degrees of thermal maturity. However, the extremely strong fluorescence background in CI chondrites compared to CM chondrites cannot be explained by H/C ratios of organic matter, since the H/C ratios of IOM are similar between CI and CM chondrites (0.65–0.73; Alexander et al., 2007). Although a possible relationship between fluorescence and the relative abundances of aliphatic carbon (to aromatic carbon) is discussed by Busemann et al. (2007), the peak intensities of aliphatic carbon in the FTIR spectra of Ryugu intact grains are comparable with those of types 1 and 2 chondrites, or even lower (Yabuta et al., 2023). The synchrotron mid- to far-infrared spectroscopic study by Dartois et al. (2023) showed that Ryugu particles have higher CH₂/CH₃ peak intensity ratios than CI chondrites, whereas their ratios are similar to the range observed among type 2 and 3 chondrites. If the high fluorescence background is solely derived from the abundance ratio of CH₂/CH₃, Ryugu particles should have fluorescence intensities as low as those of type 2 chondrites. However, the fluorescence intensities from the Ryugu particles are higher than in type 2 chondrites and lower than type 1 chondrites (240 μW). Thus, it is unlikely that CH₂/CH₃ ratio is the only cause of the strong fluorescence in Ryugu particles.

Abundance of Macromolecular Organic Matter

Initial chemical analysis of Ryugu particles indicated that Ryugu particles contain higher amount of carbon than Ivuna due to high abundance of carbonate minerals in Ryugu (Naraoka et al., 2023; Yokoyama et al., 2022). Raman spectra in this study were collected from the fine-grained matrix area of Ryugu particles and carbonaceous chondrites. Considering the total carbon content reflects the abundance of carbonate grains, it is not reasonable to assume that there is a direct relation between the fluorescence intensity of point analysis Raman spectra and bulk carbon content. Rather, the fluorescence intensity is likely reflecting the amount of organic matter contained in their matrices of the analyzed spot. Indeed, the total organic carbon content of Ryugu is similar to CI chondrite Ivuna (both samples contain ~3.0 wt% based on Yokoyama et al., 2022). Since Ryugu and CI chondrites are mainly composed of matrices, the relative abundance of organic carbon in the matrix should be similar to organic carbon contents. Similarities in total organic carbon contents of Ryugu and CI chondrites are consistent with the similar fluorescence intensities observed from both types of samples.

Organic carbon in carbonaceous chondrites and asteroid Ryugu samples can be divided into soluble and insoluble fractions. We argue here that IOM makes a major contribution to the fluorescence intensity. In support of this argument, it should be noted that fluorescence intensities typically observed in unheated type 2 chondrites are fairly similar to those of heated type 2 chondrites (i.e., Jbilet Winselwan). In general, SOM in heated type 2 chondrites is depleted compared to the unheated type 2 chondrites (e.g., Shimoyama et al., 1989). It has been reported that the relative abundance of soluble polycyclic aromatic hydrocarbons in Jbilet Winselwan is three orders of magnitude less than in the unheated Murray meteorite (Kato & Yabuta, 2019). These results indicate that the contribution of SOM to the fluorescence is small compared to the effect of IOM. Based on this idea, the difference in fluorescence intensities between type 1 and 2 chondrites could be related to the difference in the ratios of IOM to SOM. The bulk IOM contents reported for CI and CM chondrites are CI (~2 wt%) > unheated CM (~1 wt%) (Alexander et al., 2007). Although the total contents of SOM are unknown, amino acid concentrations determined in type 1 chondrites (Burton et al., 2014; Ehrenfreund et al., 2001) are one order of magnitude less than those in type 2 chondrites (e.g., Glavin et al., 2010). Thus, the higher IOM/SOM ratios appear to correlate with the significantly high fluorescence background in type 1 chondrites. Considering that the SOM contents in Ryugu samples are as low as or lower than those in the type 1 chondrites (Naraoka et al., 2023), it is similarly

the relative abundances of IOM that contributes to the high fluorescence background in Ryugu.

TEM observation of Ryugu particles has revealed that most of the organic matter in Ryugu is present as nanoparticles, nanoglobules, and diffuse carbon intercalated into phyllosilicates whose compositions are chondritic IOM-like or more aromatic (Stroud et al., 2024; Yabuta et al., 2023). It is very likely that these geometries-bearing macromolecules could limit the reabsorption of photons, resulting in a high fluorescence intensity in their Raman spectra. The natural geometries, compositions, and distributions of macromolecular organic matter in the intact Ryugu particles are partially altered in the acid-extracted residues of Ryugu, which caused differences in their fluorescence intensities (Table 1).

CONCLUSIONS

We have used Raman spectroscopy to analyze the organic structures and the degree of thermal processing of Ryugu particles and their extracted carbonaceous residues. The main conclusions are as follows:

- i. Ryugu particles and their extracted residue are characterized by a superimposed laser-induced fluorescence background in their Raman spectra. The Raman parameters of D and G bands of the Ryugu particles are similar to those of the CI and unheated CM chondrites and are distinct from those of the type 3 chondrites. This observation indicates that the surface materials of Ryugu have escaped long-duration thermal metamorphism, which is consistent with Bonal et al. (2024) as well as other results derived from chemical and mineralogical studies of Ryugu particles (Nakamura et al., 2022; Yokoyama et al., 2022).
- ii. The high fluorescence signatures of Ryugu particles show similarities to the Raman spectra observed in CI chondrites, strengthening the link with CI chondrites, and distinguishing the Ryugu particles from type 2 and 3 chondrites. The observed fluorescence signatures are consistent with the low degree of thermal maturity of the organic matter, supporting the evidence that Ryugu particles have escaped significant parent body thermal metamorphism.
- iii. The high fluorescence background intensities of the Ryugu particles result from multiple causes, but it is likely that high relative abundances of macromolecular organic matter (IOM) in total organic carbon make large contributions to the fluorescence intensities. Locally observed high fluorescence in the acid-extracted residues of Ryugu is due to nitrogen-bearing functional chemistry. The high fluorescence signature is one consequence of

the low degree of thermal maturity of the organic matter and supports evidence that the Ryugu particles have escaped significant parent body thermal metamorphism.

Acknowledgments—We thank Natsuhiko Sugimura, Midori Tanaka, and Takahiro Goto for technical assistance at the Material Characterization Central Laboratory, Waseda University. We thank Henner Busemann and the anonymous reviewer for their constructive comments during the review process and Timothy Jull for editorial handling. We acknowledge Bruno Fectay and Carine Bidaut for providing carbonaceous chondrite samples of Tagish Lake and Tarda. M.K. was supported by the Japan Society for the Promotion of Science KAKENHI (grant number JP23K03479).

Data Availability Statement—The data that support the findings of this study are available in the supplementary material of this article.

Editorial Handling—Dr. A. J. Timothy Jull

REFERENCES

- Alexander, C. M. O'D., Cody, G. D., De Gregorio, B. T., Nittler, L. R., and Stroud, R. M. 2017. The Nature, Origin and Modification of Insoluble Organic Matter in Chondrites, the Major Source of Earth's C and N. *Chemie der Erde-Geochemistry* 77: 227–256. <https://doi.org/10.1016/j.chemer.2017.01.007>.
- Alexander, C. M. O'D., Fogel, M., Yabuta, H., and Cody, G. D. 2007. The Origin and Evolution of Chondrites Recorded in the Elemental and Isotopic Compositions of their Macromolecular Organic Matter. *Geochimica et Cosmochimica Acta* 71: 4380–4403. <https://doi.org/10.1016/j.gca.2007.06.052>.
- Amano, K., Matsuoka, M., Nakamura, T., Kagawa, E., Fujioka, Y., Potin, S. M., Hiroi, T., et al. 2023. Reassigning CI Chondrite Parent Bodies Based on Reflectance Spectroscopy of Samples from Carbonaceous Asteroid Ryugu and Meteorites. *Science Advances* 9: eadi3789. <https://doi.org/10.1126/sciadv.adi3789>.
- Arakawa, M., Saiki, T., Wada, K., Ogawa, K., Kadono, T., Shirai, K., Sawada, H., et al. 2020. An Artificial Impact on the Asteroid 162173 Ryugu Formed a Crater in the Gravity-Dominated Regime. *Science* 368: 67–71. <https://doi.org/10.1126/science.aaz1701>.
- Beyssac, O., Goffe', B., Petitet, J.-P., Froigneux, E., Moreau, M., and Rouzaud, J.-N. 2003. On the Characterization of Disordered and Heterogeneous Carbonaceous Materials by Raman Spectroscopy. *Spectrochimica Acta Part A* 59: 2267–76.
- Bonal, L., Bourot-Denise, M., Quirico, E., Montagnac, G., and Lewin, E. 2007. Organic Matter and Metamorphic History of CO Chondrites. *Geochimica et Cosmochimica Acta* 71: 1605–23. <https://doi.org/10.1016/j.gca.2006.12.014>.
- Bonal, L., Gattacceca, J., Garenne, A., Eschrig, J., Rochette, P., and Ruggiu, L. K. 2020. Water and Heat: New Constraints on the Evolution of the CV Chondrite Parent Body. *Geochimica et Cosmochimica Acta* 276: 363–383. <https://doi.org/10.1016/j.gca.2020.03.009>.
- Bonal, L., Quirico, E., Bourot-Denise, M., and Montagnac, G. 2006. Determination of the Petrologic Type of CV3 Chondrites by Raman Spectroscopy of Included Organic Matter. *Geochimica et Cosmochimica Acta* 70: 1849–63. <https://doi.org/10.1016/j.gca.2005.12.004>.
- Bonal, L., Quirico, E., Flandinet, L., and Montagnac, G. 2016. Thermal History of Type 3 Chondrites from the Antarctic Meteorite Collection Determined by Raman Spectroscopy of their Polyaromatic Carbonaceous Matter. *Geochimica et Cosmochimica Acta* 189: 312–337. <https://doi.org/10.1016/j.gca.2016.06.017>.
- Bonal, L., Quirico, E., Montagnac, G., Komatsu, M., Kebukawa, Y., Yabuta, H., Amano, K., et al. 2024. The Thermal History of Ryugu Based on Raman Characterization of Hayabusa2 Samples. *Icarus* 408: 115826. <https://doi.org/10.1016/j.icarus.2023.115826>.
- Brearley, A. J. 2006. The Action of Water. In *Meteorites and the Early Solar System II*, edited by D. S. Lauretta, and H. Y. McSween, Jr., 584. Tucson, AZ: The University of Arizona Press.
- Burton, A. S., Grunsfeld, S., Elsila, J. E., Glavin, D. P., and Dworkin, J. P. 2014. The Effects of Parent-Body Hydrothermal Heating on Amino Acid Abundances in CI-Like Chondrites. *Polar Science* 8: 255–263.
- Busemann, H., Alexander, C. M. O'D., and Nittler, L. R. 2007. Characterization of Insoluble Organic Matter in Primitive Meteorites by microRaman Spectroscopy. *Meteoritics & Planetary Science* 42: 1387–1416. <https://doi.org/10.1111/j.1945-5100.2007.tb00581.x>.
- Dartois, E., Kebukawa, Y., Yabuta, H., Mathurin, J., Engrand, C., Duprat, J., Bejach, L., et al. 2023. Chemical Composition of Carbonaceous Asteroid Ryugu from Synchrotron Spectroscopy in the Mid- to Far-Infrared of Hayabusa2-Returned Samples. *Astronomy & Astrophysics* 671: A2. <https://doi.org/10.1051/0004-6361/202244702>.
- Ehrenfreund, P., Glavin, D. P., Botta, O., Cooper, G., and Bada, J. L. 2001. Extraterrestrial Amino Acids in Orgueil and Ivuna: Tracing the Parent Body of CI Type Carbonaceous Chondrites. *Proceedings of the National Academy of Sciences of the United States of America* 98: 2138–41.
- Ferrari, A., and Robertson, J. 2000. Interpretation of Raman Spectra of Disordered and Amorphous Carbon. *Physical Review B: Condensed Matter and Materials Physics* 61: 14095–107. <https://doi.org/10.1103/PhysRevB.61.14095>.
- Friend, P., Hezel, D. C., Barrat, J.-A., Jutta Zipfel, J., Palme, H., and Metzler, K. 2018. Composition, Petrology, and Chondrule-Matrix Complementarity of the Recently Discovered Jbilet Winselwan CM2 Chondrite. *Meteoritics & Planetary Science* 53: 2470–91. <https://doi.org/10.1111/maps.13139>.
- Fujiya, W., Higashi, H., Hibiya, Y., Sugawara, S., Yamaguchi, A., Kimura, M., and Hashizume, K. 2022. Hydrothermal Activities on C-Complex Asteroids Induced by Radioactivity. *The Astrophysical Journal Letters* 924: L16.
- Glavin, D. P., Michael, P., Callahan, M. P., Dworkin, J. P., and Elsila, J. E. 2010. The Effects of Parent Body Processes on Amino Acids in Carbonaceous Chondrites.

- Meteoritics & Planetary Science* 45: 1948–72. <https://doi.org/10.1111/j.1945-5100.2010.01132.x>.
- Homma, Y., Kouketsu, Y., Kagi, H., Mikouchi, T., and Yabuta, H. 2015. Raman Spectroscopic Thermometry of Carbonaceous Material in Chondrites: Four-Band Fitting Analysis and Expansion of Lower Temperature Limit. *Journal of Mineralogical and Petrological Sciences* 110: 276–282.
- Kato, H., and Yabuta, H. 2019. Polycyclic Aromatic Hydrocarbons and Aliphatic Hydrocarbons in Jbilet Winselwan Carbonaceous CM Chondrite, a Possible Analog of Asteroid Ryugu's Surface. 82nd Annual Meeting of the Meteoritical Society. LPI Contribution no. 2157.
- Kebukawa, Y., Quirico, E., Dartois, E., Yabuta, H., Bejach, L., Bonal, L., Dazzi, A., et al. 2023. Infrared Absorption Spectra from Organic Matter in the Asteroid Ryugu Samples: Some Unique Properties Compared to Unheated Carbonaceous Chondrites. *Meteoritics & Planetary Science* in press. <https://doi.org/10.1111/maps.14064>
- King, A. J., Russel, S. S., Schofield, P. F., Humphreys-Williams, E. R., Strekopytov, S., Abernethy, F. A. J., Verchovsky, A. B., et al. 2019. The Alteration History of the Jbilet Winselwan CM Carbonaceous Chondrite: An Analog for C-Type Asteroid Sample Return. *Meteoritics & Planetary Science* 54: 521–543. <https://doi.org/10.1111/maps.13224>.
- Kitazato, K., Milliken, R. E., Iwata, T., Abe, M., Ohtake, M., Matsuura, S., Arai, T., et al. 2019. The Surface Composition of Asteroid 162173 Ryugu from Hayabusa2 near-Infrared Spectroscopy. *Science* 364: 272–75. <https://doi.org/10.1126/science.aav7432>.
- Kouketsu, Y., Mizukami, T., Mori, H., Endo, S., Aoya, M., Hara, H., Nakamura, D., and Wallis, S. 2014. A New Approach to Develop the Raman Carbonaceous Material Geothermometer for Low-Grade Metamorphism Using Peak Width. *Island Arc* 23: 33–50.
- Krot, A. N., Scott, E. R. D., and Zolensky, M. 1995. Mineralogical and Chemical Modification of Components in CV3 Chondrites: Nebular or Asteroidal Processing? *Meteoritics* 30: 748–775.
- Lauretta, D. S., Adam, C. D., Allen, A. J., Ballouz, R.-L., Barnouin, O. S., Becker, K. J., Becker, T., et al. 2022. Spacecraft Sample Collection and Subsurface Excavation of Asteroid (101955) Bennu. *Science* 377: 285–291. <https://doi.org/10.1126/science.abm1018>.
- Lentfort, S., Bischoff, A., Ebert, S., and Patzek, M. 2021. Classification of CM Chondrite Breccias—Implications for Evaluation of Samples from the OSIRIS-rex and Hayabusa 2 Missions. *Meteoritics & Planetary Science* 56: 127–147.
- Muñoz Caro, G. M., Matrajt, G., Dartois, E., Nuevo, M., d'Hendecourt, L., Deboffe, D., Montagnac, G., Chauvin, N., Boukari, C., and Le du, D. 2006. Nature and Evolution of the Dominant Carbonaceous Matter in Interplanetary Dust Particles: Effects of Irradiation and Identification with a Type of Amorphous Carbon. *Astronomy & Astrophysics* 459: 147–159. <https://doi.org/10.1051/0004-6361:20042571>.
- Nakamura, T. 2005. Post-Hydration Thermal Metamorphism of Carbonaceous Chondrites. *Journal of Mineralogical and Petrological Sciences* 100: 260–272. <https://doi.org/10.2465/jmps.100.260>.
- Nakamura, T., Matsumoto, M., Amano, K., Enokido, Y., Zolensky, M. E., Mikouchi, T., Genda, H., et al. 2022. Formation and Evolution of Carbonaceous Asteroid Ryugu: Direct Evidence from Returned Samples. *Science* 379: eabn8671. <https://doi.org/10.1126/science.abn8671>.
- Naraoka, H., Takano, Y., Dworkin, J. P., Oba, Y., Hamase, K., Furusho, A., Ogawa, N. O., et al. 2023. Soluble Organic Molecules in Samples of the Carbonaceous Asteroid (162173) Ryugu. *Science* 379: eabn9033. <https://doi.org/10.1126/science.abo043>.
- Noguchi, T., Matsumoto, T., Miyake, A., Igami, Y., Haruta, M., Saito, H., Hata, S., et al. 2023. Mineralogy and Petrology of Fine-Grained Samples Recovered from the Asteroid (162173) Ryugu. *Meteoritics & Planetary Science* in press. <https://doi.org/10.1111/maps.14093>.
- Noguchi, T., Matsumoto, T., Miyake, A., Igami, Y., Haruta, M., Saito, H., Hata, S., et al. 2023. A Dehydrated Space-Weathered Skin Cloaking the Hydrated Interior of Ryugu. *Nature Astronomy* 7: 170–181. <https://doi.org/10.1038/s41550-022-01841-6>.
- Okazaki, R., Marty, B., Busemann, H., Hashizume, K., Gilmour, J. D., Meshik, A., Yada, T., et al. 2022. Noble Gases and Nitrogen in Samples of Asteroid Ryugu Record its Volatile Sources and Recent Surface Evolution. *Science* 379: 788. <https://doi.org/10.1126/science.abo043>.
- Quirico, E., Bonal, L., Beck, P., Alexander, C. M. O'D., Yabuta, H., Nakamura, T., Nakato, A., et al. 2018. Prevalence and Nature of Heating Processes in CM and C2-Untergrouped Chondrites as Revealed by Insoluble Organic Matter. *Geochimica et Cosmochimica Acta* 241: 17–37. <https://doi.org/10.1016/j.gca.2018.08.029>.
- Quirico, E., Bonal, L., Kebukawa, Y., Amano, K., Yabuta, H., Phan, V. T. H., Beck, P., et al. 2023. Compositional Heterogeneity of Insoluble Organic Matter Extracted from Hayabusa2 Samples. *Meteoritics & Planetary Science* in press. <https://doi.org/10.1111/maps.14097>.
- Quirico, E., Borg, J., Raynal, P.-I., Montagnac, G., and d'Hendecourt, L. 2005. A Micro-Raman Survey of 10 IDPs and 6 Carbonaceous Chondrites. *Planetary and Space Science* 53: 1443–48.
- Quirico, E., Montagnac, G., Rouzaud, J.-N., Bonal, L., Bourot-Denise, M., Duber, S., and Reynard, B. 2009. Precursor and Metamorphic Condition Effects on Raman Spectra of Poorly Ordered Carbonaceous Matter in Chondrites and Coals. *Earth and Planetary Science Letters* 287: 185–193.
- Quirico, E., Orthous-Daunay, F.-R., Beck, P., Bonal, L., Brunetto, R., Dartois, E., Pino, T., et al. 2014. Origin of Insoluble Organic Matter in Type 1 and 2 Chondrites: New Clues, New Questions. *Geochimica et Cosmochimica Acta* 136: 89–99.
- Quirico, E., Raynal, P.-I., and Bourot-Denise, M. 2003. Metamorphic Grade of Organic Matter in Six Unequilibrated Ordinary Chondrites. *Meteoritics & Planetary Science* 38: 795–811. <https://doi.org/10.1111/j.1945-5100.2003.tb00043.x>.
- Quirico, E., Rouzaud, J.-N., Bonal, L., and Montagnac, G. 2005. Maturation Grade of Coals as Revealed by Raman Spectroscopy: Progress and Problems. *Spectrochimica Acta Part A* 61: 2368–77.
- Shimoyama, A., Naraoka, H., Komiya, M., and Harada, K. 1989. Analyses of Carboxylic Acids and Hydrocarbons in Antarctic Carbonaceous Chondrites, Yamato-74662 and Yamato-793321. *Geochemical Journal* 23: 181–193.

- Starkey, N. A., Franchi, I. A., and Alexander, C. M. O'D. 2013. A Raman Spectroscopic Study of Organic Matter in Interplanetary Dust Particles and Meteorites Using Multiple Wavelength Laser Excitation. *Meteoritics & Planetary Science* 48: 1800–1822. <https://doi.org/10.1111/maps.12196>.
- Stroud, R., Barosch, J., Bonal, L., Burgess, K., Cody, G., De Gregorio, B., Daly, L., et al. 2024. Electron Microscopy Observations of the Diversity of Ryugu Organic Matter and its Relationship to Minerals at the Micro-to-Nanoscale. *Meteoritics & Planetary Science* in press. <https://doi.org/10.1111/maps.141281>.
- Sugita, S., Honda, R., Morota, T., Kameda, S., Sawada, H., Tatsumi, E., Yamada, M., et al. 2019. The Geomorphology, Color, and Thermal Properties of Ryugu: Implications for Parent-Body Processes. *Science* 364: eaaw0422. <https://doi.org/10.1126/science.aaw0422>.
- Tachibana, S., Sawada, H., Okazaki, R., Takano, Y., Sakamoto, K., Miura, Y. N., Okamoto, C., et al. 2022. Pebbles and Sand on Asteroid (162173) Ryugu: In Situ Observation and Particles Returned to Earth. *Science* 375: 1011–16. <https://doi.org/10.1126/science.abj8624>.
- Tsuda, Y., Saiki, T., Terui, F., Nakazawa, S., Yoshikawa, M., Watanabe, S., and Hayabusa2 Project Team. 2020. Hayabusa2 Mission Status: Landing, Roving and Cratering on Asteroid Ryugu. *Acta Astronautica* 171: 42–54. <https://doi.org/10.1016/j.actaastro.2020.02.035>.
- Velbel, M. A., and Zolensky, M. E. 2021. Thermal Metamorphism of CM Chondrites: A Dihydroxylation-Based Peak-Temperature Thermometer and Implication for Sample Return from Asteroids Ryugu and Bennu. *Meteoritics & Planetary Science* 56: 546–585.
- Watanabe, S., Hirabayashi, M., Hirata, N., Hirata, N., Noguchi, R., Shimaki, Y., Ikeda, H., et al. 2019. Hayabusa2 Arrives at the Carbonaceous Asteroid 162173 Ryugu—A Spinning Top-Shaped Rubble Pile. *Science* 364: 268–272. <https://doi.org/10.1126/science.aav8032>.
- Wopenka, B. 1988. Raman Observations on Individual Interplanetary Dust Particles. *Earth and Planetary Science Letters* 88: 221–231.
- Wopenka, B., Xu, Y. C., Zinner, E., and Amari, S. 2013. Murchison Presolar Carbon Grains of Different Density Fractions: A Raman Spectroscopic Perspective. *Geochimica et Cosmochimica Acta* 106: 463–489.
- Yabuta, H., Cody, G. D., Engrand, C., Kebukawa, Y., De Gregorio, B., Bonal, L., Remusat, L., et al. 2023. Macromolecular Organic Matter in Samples of the Asteroid (162173) Ryugu. *Science* 379: abn9057. <https://doi.org/10.1126/science.abn9057>.
- Yada, T., Abe, M., Okada, T., Nakato, A., Yogata, K., Miyazaki, A., Hatakeda, K., et al. 2022. Preliminary Analysis of the Hayabusa2 Samples Returned from C-Type Asteroid Ryugu. *Nature Astronomy* 6: 214–220. <https://doi.org/10.1038/s41550-021-01550-6>.
- Yokoyama, T., Nagashima, K., Nakai, I., Young, E. D., Abe, Y., Aléon, J., Alexander, C. M. O'D., et al. 2022. Samples Returned from the Asteroid Ryugu Are Similar to Ivuna-Type Carbonaceous Meteorites. *Science* 379: abn7850. <https://doi.org/10.1126/science.abn7850>.

SUPPORTING INFORMATION

Additional supporting information may be found in the online version of this article.

Data S1. Effects of laser power on Raman spectra, supplementary figures of Raman parameters to compare

the values obtained by teams from Japan and France, comparison of Raman parameters for the surface and interior of a single particle, and a table of Raman parameters of Ryugu and meteorites measured at 240 μ W.